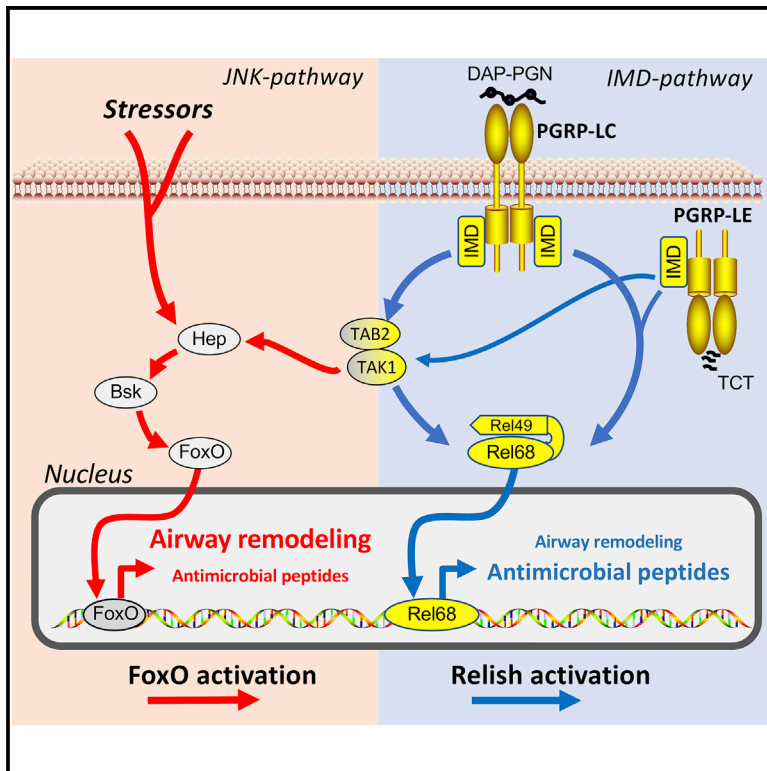# eScholarship@UMassChan

Constitutive immune activity promotes JNK- and FoxO-dependent remodeling of Drosophila airways

Item Type	Journal Article
Authors	Wagner, Christina;Silverman, Neal;Roeder, Thomas
Citation	Wagner C, Uliczka K, Bossen J, Niu X, Fink C, Thiedmann M, Knop M, Vock C, Abdelsadik A, Zissler UM, Isermann K, Garn H, Pieper M, Wegmann M, Koczulla AR, Vogelmeier CF, Schmidt-Weber CB, Fehrenbach H, König P, Silverman N, Renz H, Pfefferle P, Heine H, Roeder T. Constitutive immune activity promotes JNK- and FoxO-dependent remodeling of Drosophila airways. Cell Rep. 2021 Apr 6;35(1):108956. doi: 10.1016/j.celrep.2021.108956. PMID: 33826881. Link to article on publisher's site
DOI	10.1016/j.celrep.2021.108956
Rights	Copyright 2021 The Author(s). This is an open access article under the CC BY license (http://creativecommons.org/licenses/by/4.0/).
Download date	2024-12-31 07:04:41
Item License	http://creativecommons.org/licenses/by/4.0/
Link to Item	https://hdl.handle.net/20.500.14038/41869

Constitutive immune activity promotes JNK- and FoxO-dependent remodeling of *Drosophila* airways

Graphical abstract

Highlights

- Chronic epithelial immune activation leads to structural changes in the airways

- Activation of JNK signaling via TAK1 mediates this airway remodeling

- FoxO acts downstream of JNK signaling in inducing this airway remodeling

- NF-κB factors are of minor relevance for this response

Authors

Christina Wagner, Karin Uliczka, Judith Bossen, ..., Petra Pfefferle, Holger Heine, Thomas Roeder

Correspondence

troeder@zoologie.uni-kiel.de

In brief

Chronic activation of the immune system in the *Drosophila* airway epithelium induces structural changes of the organ. Wagner et al. show these structural changes are mediated by a bifurcation of the IMD pathway at the level of TAK1, involving the JNK pathway and subsequent activation of the transcription factor FoxO.

CelPress

Article

Constitutive immune activity promotes JNK- and FoxO-dependent remodeling of *Drosophila* airways

Christina Wagner,[1,2,18] Karin Uliczka,[2,3,18] Judith Bossen,[1,15] Xiao Niu,[1] Christine Fink,[1] Marcus Thiedmann,[1] Mirjam Knop,[1] Christina Vock,[4] Ahmed Abdelsadik,[6,7] Ulrich M. Zissler,[8,16] Kerstin Isermann,[1] Holger Garn,[9,17] Mario Pieper,[13] Michael Wegmann,[5,15] Andreas R. Koczulla,[10,17] Claus F. Vogelmeier,[10,17] Carsten B. Schmidt-Weber,[8,16] Heinz Fehrenbach,[4,15] Peter König,[13,15] Neil Silverman,[14] Harald Renz,[11,17] Petra Pfefferle,[12,17] Holger Heine,[3,15] and Thomas Roeder[1,15,19,*]

[1]Zoology, Department of Molecular Physiology, Kiel University, 24118 Kiel, Germany
[2]Division of Invertebrate Models, Priority Research Area Asthma and Allergy, Research Center Borstel, 23845 Borstel, Germany
[3]Division of Innate Immunity, Priority Research Area Asthma and Allergy, Research Center Borstel, 23845 Borstel, Germany
[4]Division of Experimental Pneumology, Priority Research Area Asthma and Allergy, Research Center Borstel, 23845 Borstel, Germany
[5]Division of Asthma Exacerbation & Regulation, Priority Research Area Asthma and Allergy, Research Center Borstel, 23845 Borstel, Germany
[6]Zoology, Aswan University, Aswan 81528, Egypt
[7]Molecular Biotechnology Program, Faculty of Advanced Basic Sciences, Galala University, 43552 New Galala, Egypt
[8]Center of Allergy and Environment (ZAUM), Technical University Munich and Helmholtz Center Munich, German Research Center for Environmental Health, 80802 Munich, Germany
[9]Translational Inflammation Research Division & Core Facility for Single Cell Multiomics, Medical Faculty, Philipps University of Marburg, 35043 Marburg, Germany
[10]Pulmonary and Critical Care Medicine, Department of Medicine, Medical Faculty, Philipps University of Marburg, 35043 Marburg, Germany
[11]Molecular Diagnostics, Institute of Laboratory Medicine and Pathobiochemistry, Medical Faculty, Philipps University of Marburg, 35043 Marburg, Germany
[12]Comprehensive Biobank Marburg, University Medical Center Giessen and Marburg, Medical Faculty, Philipps University Marburg, 35043 Marburg, Germany
[13]University Lübeck, Anatomical Institute, 23538 Lübeck, Germany
[14]University of Massachusetts Medical School, Worcester, MA 01605, USA
[15]Airway Research Center North (ARCN), Member of the German Center for Lung Research (DZL), Grosshansdorf, Germany
[16]CPC-M, Member of the German Center for Lung Research (DZL), Munich, Germany
[17]UGMLC, Member of the German Center for Lung Research (DZL), Marburg, Germany
[18]These authors contributed equally
[19]Lead contact
*Correspondence: troeder@zoologie.uni-kiel.de
https://doi.org/10.1016/j.celrep.2021.108956

SUMMARY

Extensive remodeling of the airways is a major characteristic of chronic inflammatory lung diseases such as asthma or chronic obstructive pulmonary disease (COPD). To elucidate the importance of a deregulated immune response in the airways for remodeling processes, we established a matching *Drosophila* model. Here, triggering the Imd (immune deficiency) pathway in tracheal cells induced organ-wide remodeling. This structural remodeling comprises disorganization of epithelial structures and comprehensive epithelial thickening. We show that these structural changes do not depend on the Imd pathway's canonical branch terminating on nuclear factor κB (NF-κB) activation. Instead, activation of a different segment of the Imd pathway that branches off downstream of Tak1 and comprises activation of c-Jun N-terminal kinase (JNK) and forkhead transcription factor of the O subgroup (FoxO) signaling is necessary and sufficient to mediate the observed structural changes of the airways. Our findings imply that targeting JNK and FoxO signaling in the airways could be a promising strategy to interfere with disease-associated airway remodeling processes.

INTRODUCTION

Airway epithelial cells not only constitute the first line of defense against airborne pathogens but are also pivotal for maintaining the lung's structural integrity and immune homeostasis (Lambrecht and Hammad, 2012; Proud and Leigh, 2011; Whitsett and Alenghat, 2015). The airway epithelium functions as a sentinel, translating external and internal information into physiological or pathophysiological responses. Chronic epithelial disorders of the lung, such as asthma,

COPD (chronic obstructive pulmonary disease), and cystic and pulmonary fibrosis, are associated with inflammation and structural remodeling (Adam et al., 2015; Camelo et al., 2014; Hiemstra et al., 2015; Holgate, 2007a; Whitsett and Alenghat, 2015). In particular, deregulated epithelial immune homeostasis appears to be involved in most of these diseases (Proud and Leigh, 2011; Van Eerdewegh et al., 2002; Wark et al., 2005).

Most components of the airway innate immune system converge onto nuclear factor κB (NF-κB) activation; chronic deregulation of this signaling pathway is associated with development of a number of chronic lung diseases (Broide, 2008; Broide et al., 2005; Cheng et al., 2007; Hart et al., 1998; Pantano et al., 2008). NF-κB signaling in airway epithelial cells not only regulates the expression of proinflammatory cytokines and antimicrobial peptides but has also been shown to be involved in structural remodeling processes of the entire lung, including goblet cell hyperplasia and dedifferentiation of epithelial cells (Broide et al., 2005; Pantano et al., 2008).

To better understand the molecular basis of these structural changes, simple models are ideal. In recent years, the fruit fly *Drosophila* has been established successfully as a genetically tractable model to study the molecular framework underlying various chronic lung diseases, such as asthma, COPD, and lung cancer (Levine and Cagan, 2016; Pandey and Nichols, 2011; Prange et al., 2018; Roeder et al., 2012; Wagner et al., 2009). Insects possess a very simple, purely epithelial airway system that nevertheless shares surprising commonalities with the human lung in terms of structure, physiology, organogenesis, and innate immune system (Roeder et al., 2009). In particular, exposure of *Drosophila* airway epithelial cells to bacterial compounds and substances acting as allergens in humans induces a cell-autonomous immune response that converges on NF-κB activation (Onfelt Tingvall et al., 2001; Tzou et al., 2000; Wagner et al., 2009; Warmbold et al., 2013). However, unlike in humans, where two signaling pathways the Toll-like receptor (TLR)/interleukin-1 (IL-1) and tumor necrosis factor alpha (TNF-α) pathways, act in parallel to mediate epithelial immune responses, in the fruit fly's airway epithelium, only the immune deficiency (Imd) pathway (homologous to the mammalian TNF-α pathway) appears to be operative (Akhouayri et al., 2011; Wagner et al., 2008). Imd activation induces a powerful antimicrobial response mediated by induced expression of antimicrobial peptides (Hanson et al., 2019; Tzou et al., 2000). Moreover, local structural changes have been observed upon strong antimicrobial responses to infection in the airways of *Drosophila* (Wagner et al., 2009).

However, the mechanisms by which constitutive activation of the airway epithelial immune response results in pathologic tissue remodeling are not well understood. To address this question, we specifically activated the Imd pathway in *Drosophila* airways and then analyzed the functional and structural consequences. We show that activation of epithelial immunity through the Imd pathway induces strong airway remodeling comprising epithelial meta- and hyperplasia. Surprisingly, this reaction does not depend on the canonical branch of the Imd pathway leading to NF-κB activation but on an alternative branch comprising c-Jun N-terminal kinase

(JNK) and forkhead transcription factor of the O subgroup (FoxO) signaling.

RESULTS

Constitutive Imd activation in the airway epithelium induces a strong antimicrobial response

Taking advantage of its simple airway structure and the unique and highly versatile toolbox available for *Drosophila* (Kallsen et al., 2015; Wagner et al., 2008), we studied the outcome of constitutively activated innate immune signaling in airway epithelial cells. To achieve this, we used the bipartite Gal4/upstream activating sequence (UAS) system, which allows targeted expression of the pattern recognition receptors *PGRP-LC* and *-LE* (Takehana et al., 2002) exclusively in the airways via the highly specific *ppk4*-Gal4 driver strain (Liu et al., 2003). As expected, this activation of the Imd pathway induced a significant increase in expression of all major antimicrobial peptide genes, regardless of whether *PGRP-LC* or *PGRP-LE* was used (Figure 1A).

Constitutive Imd activation leads to thickening of the airway epithelium at all life stages

Beside expression of antimicrobial peptides, the most intriguing phenotype observed in response to persistent Imd activation was thickening of the epithelial layer. This cell thickening was accompanied by loss of regularity of airway epithelial cells, resulting in fuzzy cell-cell boundaries (Figures 1B and 1C). Epithelial thickening occurred throughout the entire airway system (Figures 1D–1K, red arrowheads) with severalfold increases in thickness, regardless of whether *PGRP-LC* or *PGRP-LE* was ectopically overexpressed (Figure 1L). In these airways, the air-conducting lumen was irregular and obstructed (Figures 1I and 1K, black arrows). To exclude potential developmental effects, we used temporal refinement of the bipartite Gal4/UAS system by including the temperature-sensitive *tubP*-Gal80^ts repressor (McGuire et al., 2003). Animals carrying the *tubP*-Gal80^ts repressor in addition to the Gal4/UAS elements showed no signs of structural changes when kept at the restrictive temperature (18°C; Figure 1M, red arrowheads). In contrast, shifting first-instar larvae to the permissive temperature (28°C) for 24 h triggered a thickening of the epithelium (Figure 1N, red arrowheads), which, after 48 h culminated in the full, chronic airway remodeling phenotype (Figure 1O, red arrowheads). The most severe structural phenotypes were also associated with substantial larval lethality, leading to reduced pupation rates.

To verify whether the phenotype of thickening of the epithelia induced by Imd activation is independent of developmental processes and can be observed at all life stages, including in adults, we conducted two additional sets of experiments. To have expression control in the adult tracheal system, we used the *btl*-Gal4 driver (*btl*-Gal4, *tubP*-Gal80^ts × UAS-*PGRP-LC*) in addition to the *ppk4*-Gal4 driver already described (Figure 2). In the first experimental setup, ectopic Imd activation was restricted to the last larval stage before metamorphosis begins (L3) by shifting from the restrictive (18°C) to the permissive (28°) temperature in early L3 larvae and analyzing the phenotype at the end of this larval stage (Figure 2A). In this way, possible confounding effects caused by molting could be excluded. Here we observed an
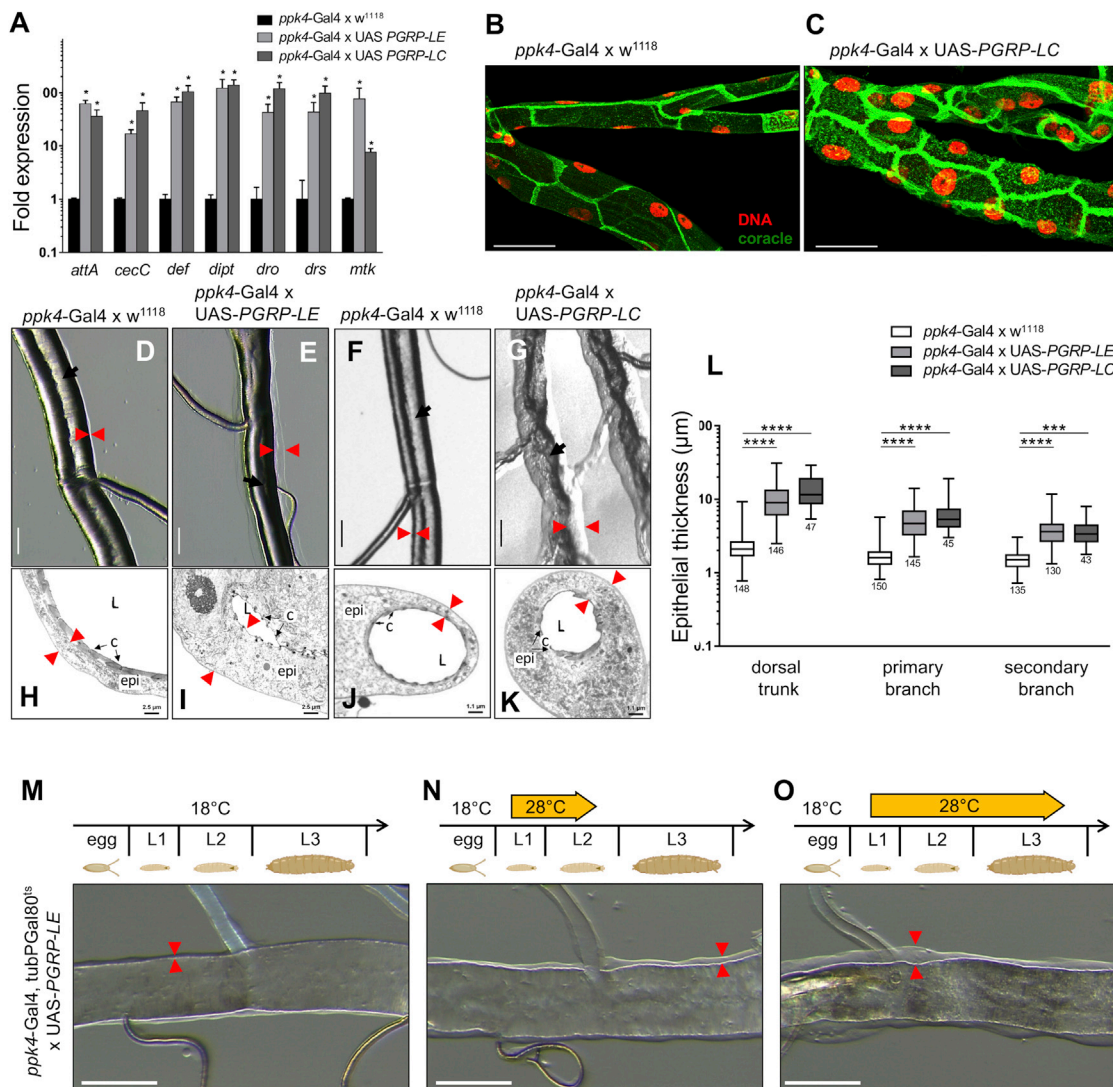
Figure 1. Constitutive activation of Imd signaling in airway epithelial cells of the fruit fly induces a strong antimicrobial response and considerable thickening of the airway epithelium across the entire airway tree

(A) Effects of ectopic Imd activation on antimicrobial peptide (AMP) gene expression in the airway epithelium of *Drosophila* larvae for airways from control animals (*ppk4*-Gal4 × *w^1118*) and animals overexpressing *PGRP-LE* (*ppk4*-Gal4 × UAS-*PGRP-LE*), and *PGRP-LC* (*ppk4*-Gal4 × UAS-*PGRP-LC*).

(B and C) Confocal fluorescence microscopy images of DAPI- and anti-coracle-stained airways (dorsal trunk and seceding primary branch) originating from control (B) and *PGRP-LC*-overexpressing larvae (C). Scale bars, 50 μm.

(D–G) Low-magnification light microscopy analyses of airways with activation of NF-κB signaling by *PGRP-LE* (E), *PGRP-LC* overexpression (G), or no activation (D and F). Red arrowheads, epithelial thickness; black arrows, inner airway lumen. Scale bars, 50 μm.

(H–K) High-resolution electron micrographs of airway branches from *PGRP-LE* (I), *PGRP-LC*-overexpressing larvae (K), or matching controls (H and J). C, cuticle; Epi, epidermis; L, lumen; black arrows, lining cuticle; red arrowheads, epithelial thickness. Scale bars, 2.5 μm.

(L) Quantification of epithelial thickness in different branching generations of airways from *PGRP-LE* (light gray bars), *PGRP-LC*-overexpressing (dark gray bars) larvae, or matching controls (white bars).

(M–O) Low-magnification light microscopy analyses of airways in which *PGRP-LE* expression was controlled temporally by the temperature-sensitive Gal4 inhibitor Gal80^ts (*ppk4*-Gal4, *tubP*-Gal80^ts, UAS-*PGRP-LC*). Shown are airways of larvae raised at 18°C (M), cultured temporarily at 28°C for 24 h (N; first > second larval instar) or 48 h (O; first > early third larval instar) after reaching the first larval instar.

Data show mean ± SEM. *p < 0.05, ***p < 0.001, ****p < 0.0001. n ≥ 3 (A, unpaired t test followed by Holm multiple comparisons testing), n ≥ 43 (L, one-way ANOVA). Scale bars, 50 μm.

almost identical phenotype as one described before (Figures 2B–2D). As expected, the non-induced controls (18°C) showed no signs of changes in airway epithelium (Figure 2b), making them

indistinguishable from wild-type controls. On the other hand, induction in early L3 larvae by shifting the animals from 18°C to 28°C induced the expected phenotype, characterized by massive
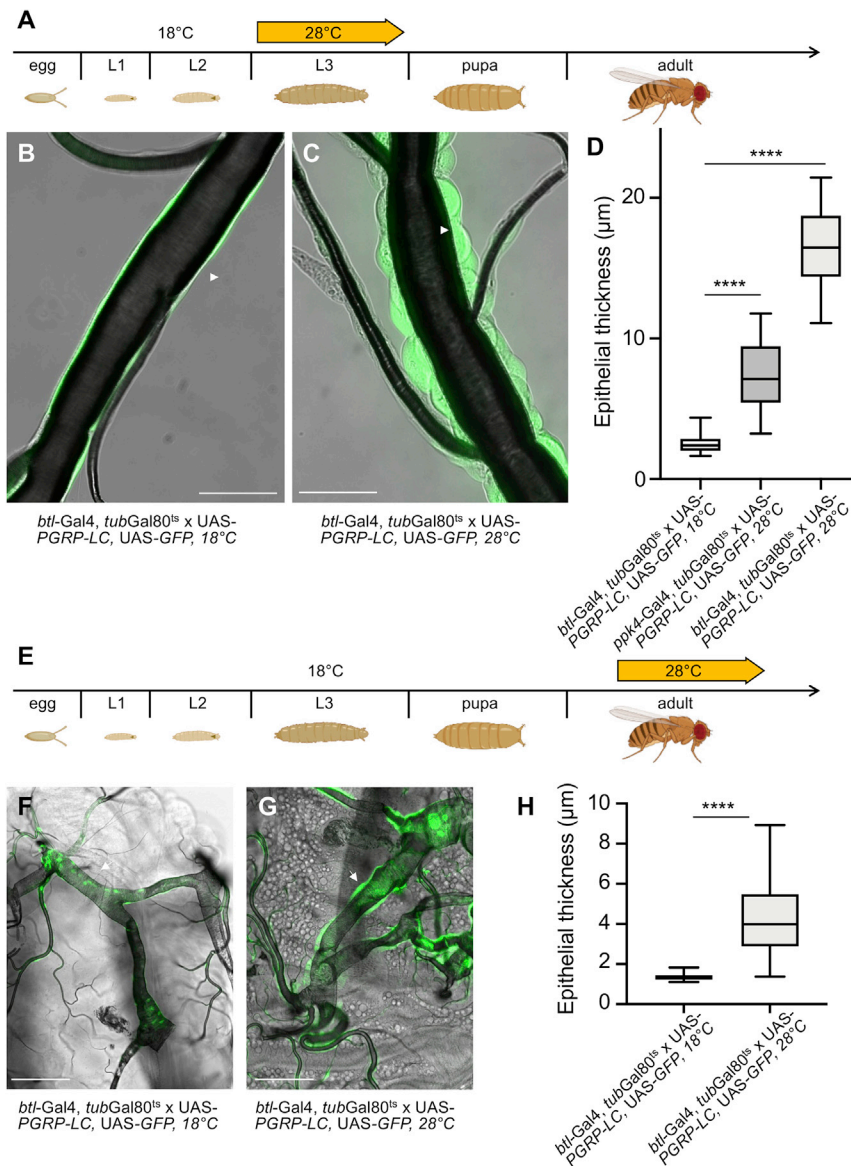
Figure 2. Imd pathway activation led to epithelial thickening even when the pathway was triggered exclusively in the last larval stage or in adults

(A) The experimental setup, showing that activation of the Imd pathway was restricted to a short phase during the last larval stage (L3).

(B and C) Control animals of the genotype (*btl*-Gal4, *tubP*-Gab80ts, UAS-*GFP*, UAS-*PGRP-LC*) were maintained at the restrictive (18°C) temperature (B), whereas experimental animals were shifted as early L3 larvae to 28°C and analyzed during the same larval stage (C).

(D) Quantitative evaluation of the thickening was done with controls (18°C), with animals shifted to the permissive temperature (28°C) for 3–4 days of the same genotype or *ppk*4-Gal4, *tubP*-Gal80^ts, UAS-*GFP*, UAS-*PGRP-LC*.

(E) Expression was restricted to the adult stage, induced by shifting the experimental animals from 18°C to 28°C in the adult stage only.

(F) In controls, animals of this genotype were kept at 18°C.

(G) For the experimental animals, a shift to 28°C was done only at the adult stage.

(H) Quantitative evaluation of airways thickness.

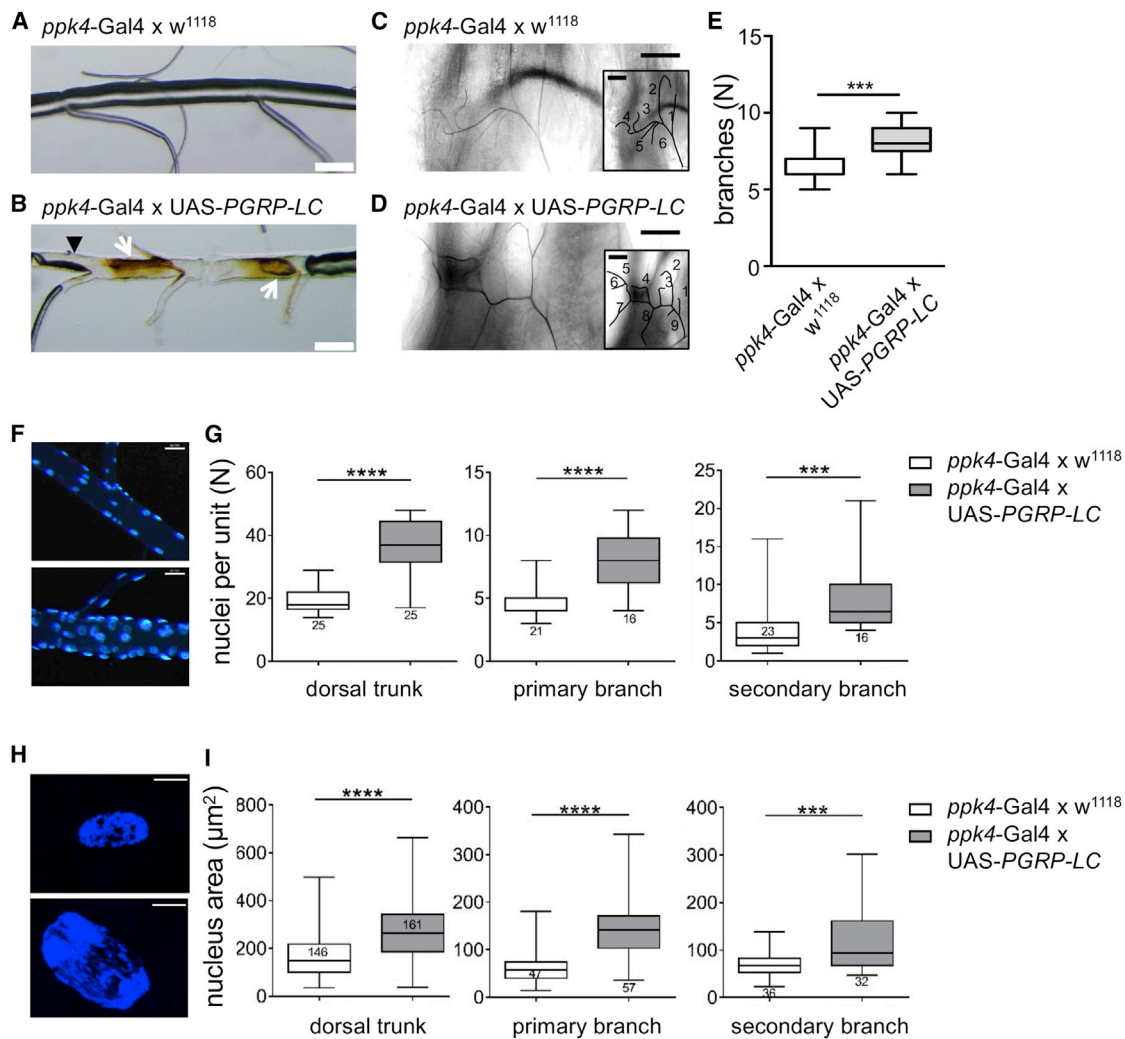n > 10, ****p < 0.0001. Scale bars, 100 μm.

we observed in larval tracheae (Figures 2G and 2H). This thickening was seen throughout the entire tracheal system and was highly significant compared with the non-induced controls (Figure 2H). These animals did not die immediately but showed substantial impairment, which included strongly reduced physical activity.

Imd activation in the airway epithelium induces meta- and hyperplasia

The persistent Imd activation in the airway epithelium that was triggered by *PGRP-LC* overexpression induced additional local changes, including partial melanization (Figure 3B, white arrows) and liquid infiltration (Figure 3B, black arrowhead). Further, larvae with airway-specific *PGRP-LC* overexpression displayed aberrant sprouting of new terminal airway branches (Figures 3D and 3E) compared with the corresponding controls (Figure 3C).

Hyperplasia (proliferation) or metaplasia (loss of epithelial cell features) could be the reason for increased epithelial thickening and a consequence of the increased amount of airway tissue. Therefore, we determined the number of nuclei per length as well as the mean nucleus area in all different branching categories of airways in which *PGRP-LC* was overexpressed. Quantification of cell numbers in *PGRP-LC*-overexpressing airways showed an increase of up to 2-fold compared with the controls, although they were still organized as a monolayer (Figures 3F and 3G). Moreover, airway epithelial nuclei of *PGRP-LC*-overexpressing airways were

thickening of the epithelium (Figure 2C). Quantitative analysis of the thickening phenotype showed that the *btl*-Gal4 driver was the more effective one. Imd activation in third-instar larvae induced thickening to similar extents compared with the induction scheme starting earlier in development, although the entire period of activation occurred during this last larval stage (Figure 2D). Finally, we induced ectopic Imd activation only in adults, avoiding any confounding influences from developmental or organ growth processes (Figure 2E). Here we used the *btl*-Gal4 driver only because the *ppk*4-Gal4 driver is active in the adult tracheal system in a very limited form. In adults, we activated the Imd pathway by shifting the animals from the restrictive (18°C) to the permissive (28°C) temperature and analyzed them 3–4 days later (Figure 2E). In non-induced controls, the airway epithelium remained normal (Figure 2F), whereas in induced ones, we observed substantial thickening of the airway epithelium that resembled the reaction

Figure 3. Imd pathway activation in the airway epithelium induced meta- and hyperplasia

(A and B) Light microscopy images of airways from control (*ppk4*-Gal4 × *w^1118*) and *PGRP-LC*-overexpressing (*ppk4*-Gal4 × *UAS-PGRP-LC*) larvae. The black arrowhead marks liquid infiltrations, and white arrows point to melanization. Scale bars, 100 μm.

(C and D) Images of terminal branches located under the epidermis of the third larval segment. Images at the bottom right show resized images in which the terminal branches were traced. Scale bars, 50 μm.

(E) Quantification of terminal branches in larvae overexpressing *PGRP-LC* (light gray bar) or in matching controls (white bar).

(F) Fluorescence images of DAPI-stained dorsal trunks originating from *PGRP-LC*-overexpressing airways (bottom image) or a matching control (top image). Scale bars, 50 μm.

(G) Quantification of cell nuclei in dorsal trunks, primary and secondary branches derived from *PGRP-LC* overexpressing airways, or matching controls.

(H) Fluorescence images of DAPI-stained nuclei from dorsal trunks of *PGRP-LC*-overexpressing airways (bottom image) or matching controls (top image). Scale bar, 10 μm.

(I) Quantification of nuclear sizes in dorsal trunks, primary and secondary branches from controls, as well as *PGRP-LC*-overexpressing airways.

Data show mean ± SEM. n ≥ 16 (E and G), n = 32 (I), two-tailed Mann-Whitney U test, ***$p < 0.001$, ****$p < 0.0001$.

at least 1.5-fold larger in size than those of airways in which *PGRP-LC* was expressed at an endogenous level (Figures 3H and 3I). Both aspects are characteristics for hyperplasia and metaplasia, which are also hallmarks of chronic inflammatory lung diseases.

Epithelial thickening triggered by Imd activation depends only to a low degree on the NF-κB factor Relish

The canonical Imd signaling cascade of *Drosophila* converges on activation of the NF-κB factor Relish, which, upon activation,

induces transcription of target genes, including those for antimicrobial peptide (Figure 4A). Although ectopic expression of a constitutively active form of Relish (*relD*) induced expression of the antimicrobial peptide (AMP) genes *drosomycin* (*drs*) and *diptericin* (*dipt*) (Figure 4B), the epithelium of *relD*-overexpressing airways was only slightly thickened compared with the ones experiencing *PGRP-LE* or *-LC* overexpression (Figure 4C; Figure S1). Subsequently, we evaluated whether Relish is necessary to induce these structural changes by ectopic overexpression of
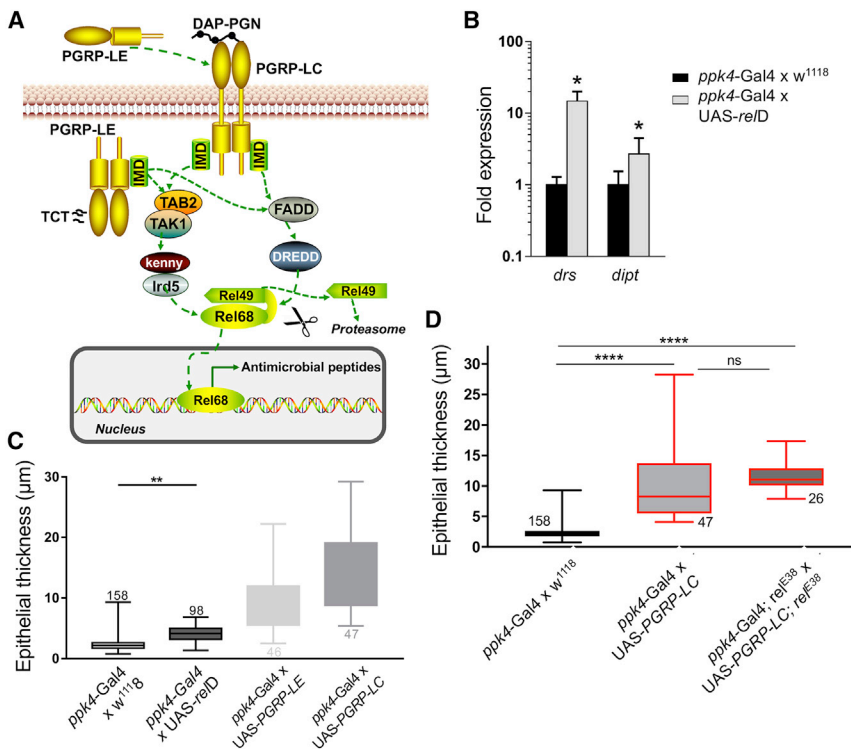
Figure 4. Epithelial thickening triggered by constitutive Imd activation depends only partially on the NF-κB transcriptional factor Relish

(A) Schematic overview of the Imd (immune deficiency) pathway. The Imd pathway is activated by the membrane-bound pattern recognition receptor *PGRP-LC* or by the soluble intracellular and/or extracellular receptor *PGRP-LE* (peptidoglycan recognition protein LC/LE). Imd activation results in phosphorylation and cleavage of the transcription factor Relish (Rel68/Rel49). Rel68 translocates into the nucleus, where it regulates the expression of AMP genes (e. g. *diptericin*). Natural elicitors of this pathway are, e.g., DAP-PGN (Diaminopimelic acid-type peptidoglycan) or TCT (tracheal cytotoxin).

(B) Quantification of *drosomycin* (*drs*) and *diptericin* (*dipt*) expression in *relD*-overexpressing and control airways from third-instar larvae.

(C) Quantitative evaluation of epithelial thickness in *relD*-overexpressing airways and matching controls. Epithelial thicknesses of *PGRP-LE-* and *PGRP-LC*-overexpressing airways are shown as gray shaded boxes and those of the other experimental analyses as gray boxes.

(D) Quantification of epithelial thicknesses in dorsal trunks of airways overexpressing *PGRP-LC* in a wild-type or a *relish*-deficient background and in matching controls. Individual numbers of analyzed animals are listed above or below the boxplots. Red-framed boxplots display the dataset for *PGRP-*

LC-overexpressing airways, dissected from larvae homozygous for the null allele *Relish^E38^*.

Data show mean ± SEM. n = 6 (B), multiple t test followed by Holm multiple comparisons testing, *p < 0.05, n ≥ 46 (C), n ≥ 20 (D), one-way ANOVA, **p < 0.01, ****p < 0.0001.

*PGRP-LC* in a *rel*-deficient background (Hedengren et al., 1999). These flies (*ppk4*-Gal4, UAS-*PGRP-LC*, *rel^38/38^*), although devoid of the Imd pathway-associated key transcription factor, developed epithelial thickening similar to animals carrying wild-type *rel* alleles (*ppk4*-Gal4, UAS-*PGRP-LC*; Figure 4D).

Imd-induced epithelial thickening relies on Tak1 and the downstream JNK signaling pathway

Because the presence of *relish* was not necessary for the airway thickening phenotype, we hypothesized that signaling routes connecting PGRP-LC activation with the JNK signaling pathway may regulate epithelial hyper- and metaplasia. Tak1, an integral part of the Imd signaling pathway, acts in concert with Tab2 to create a hub connecting the Imd with the JNK signaling pathway (Silverman et al., 2003). Thus, we examined the effect of reducing Tak1 activity by coexpression of UAS-*Tak1*-RNAi in *PGRP-LE*-overexpressing flies or coexpression of a dominant-negative Tak1 isoform (*Tak1^DN^*) in *PGRP-LC*-overexpressing ones (Figure 5A). The effects of overexpression of *PGRP-LC* or *PGRP-LE* were largely identical, so we performed the corresponding overexpression (*PGRP-LC* or *PGRP-LE*) with simultaneous reduction of Tak1 activity (RNAi or *Tak1^DN^*), depending on technical practicability. We observed a substantial reduction in epithelial thicknesses in flies overexpressing *PGRP-LE* concurrently with *Tak1*-RNAi in most parts of the tracheal system, which was significant for the primary and secondary branches but not for the dorsal

trunks (Figure 5A). The strong reduction of Tak1-dependent signaling by co-expression of *Tak1^DN^* largely reduced the increased epithelial thickness observed in *PGRP-LC*-overexpressing airways to levels that were indistinguishable from the controls for the dorsal trunks and the secondary branches (Figure 5A). This shows that *Tak1^DN^* was far more effective in reducing Tak1-mediated signaling than *Tak1*-RNAi. Because Tak1 can activate JNK signaling (Silverman et al., 2003), we tested our hypothesis that the JNK pathway is required to translate *PGRP-LE* or *PGRP-LC* activation into the structural phenotypes. Therefore, we overexpressed *PGRP-LE* concurrent with inhibiting the JNK pathway at the level of Basket (bsk; dJNK, *Drosophila* c-Jun N-terminal kinase) with two different approaches: first by using *bsk*-RNAi and second by using a dominant-negative *basket* isoform, *bsk^DN^*. This downregulation of JNK signaling by expression of *bsk*-RNAi or *bsk^DN^* concurrently with Imd pathway activation through *PGRP-LE* overexpression resulted in significantly reduced epithelial thicknesses throughout the entire airway system compared with animals where only *PGRP-LE* was overexpressed (Figure 5B; Figure S2). This reduction in induced epithelial thickening was approximately 50% on average and was statistically significant in all cases (primary and secondary branches are not shown). The lack of complete reduction of this induced phenotype might have resulted from incomplete inhibition of JNK signaling by these interventions (RNAi and *bsk^DN^*) but should also be attributed to Relish-mediated
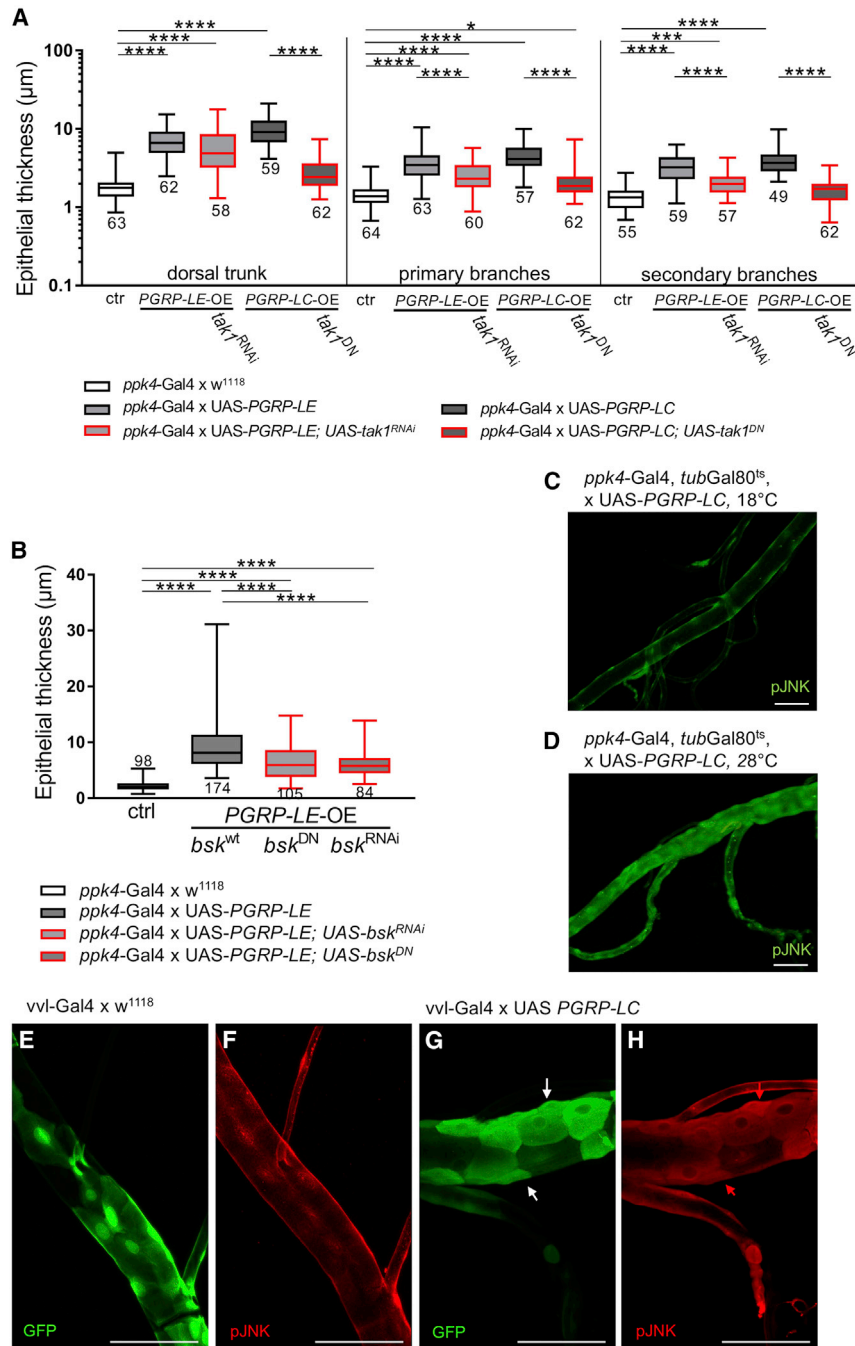
Figure 5. Imd-induced epithelial thickening depends to a major extent on the Tak1-JNK (c-Jun N-terminal kinase) axis

(A) Epithelial thicknesses of dorsal trunks (left), primary branches (center), or secondary branches (right) experiencing *PGRP-LE* or *PGRP-LC* overexpression in airway epithelial cells alone or in combination with *tak1*-RNAi or *tak1*[DN].

(B) Quantification of epithelial thicknesses in dorsal trunks of airways derived from larvae overexpressing *PGRP-LE* in a wild-type background (*w[1118]*) concurrent with a *basket* dominant-negative isoform (UAS-*bsk*[DN]) or *bsk*-RNAi (UAS-*bsk*-RNAi).

(C and D) Fluorescence images of anti-phospho-JNK (pJNK, phosphorylated JNK)-stained airways from *PGRP-LC*-overexpressing larvae (*ppk4*-Gal4/*tubP*-Gal80[ts] × UAS-*PGRP-LC*) and matching controls (*ppk4*-Gal4/*tubP*-Gal80[ts] × *w[1118]*).

(E–H) *vvl-coin*[ts] (*vvl-FLP, CoinFLP*-Gal4, UAS-*2xEGFP*/+; *tubP*-Gal80[ts])-mediated mosaic analysis of *PGRP-LC* overexpression followed by anti-pJNK immunohistochemistry. Control animals (E and F; *vvl-FLP, CoinFLP*-Gal4, UAS-*2xEGFP*/+; *tubP*-Gal80[ts] X *w[1118]*) and experimental animals (*vvl-FLP, CoinFLP-Gal4, UAS-2xEGFP*/+; *tubP*-Gal80[ts] X UAS-*PGRP-LC*), where mosaics are labeled by GFP in green (white arrows) and pJNK staining in red (red arrows), are shown. Scale bars, 100 μm (C).

Data show mean values ± SEM. n ≥ 49 (A and B), one-way ANOVA, *p < 0.05, ***p < 0.001****p < 0.0001.

the entire epithelium was seen in *PGRP-LC*-overexpressing airways (Figure 5D). To verify that the observed effects of JNK pathway activation in response to *PGRP-LC* overexpression are cell autonomous, we targeted expression to a few epithelial cells in a mosaic fashion using the *vvl*-coin system (Figures 5E–5H). In controls (*vvl*-Gal4 × *w[1118]*), staining for pJNK did not reveal any relevant signal (Figures 5E and 5F). In contrast, in mosaics where *PGRP-LC* was co-expressed in GFP-positive cells (*vvl*-Gal4 × UAS-*PGRP-LC*), we observed a strong and clear pJNK signal in cells that also express GFP (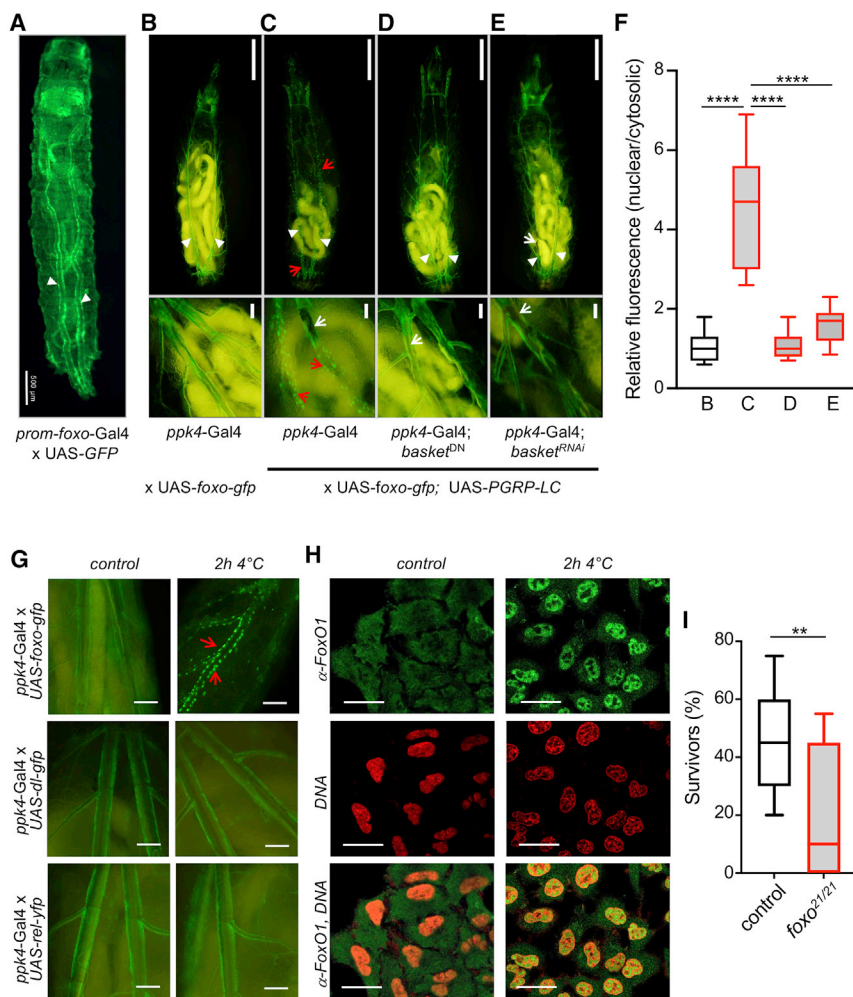Figures 5G and 5H). The lack of pJNK staining in non-affected cells shows that the effect of activation of the JNK pathway is cell autonomous.

The transcription factor FoxO is activated in the airway epithelium by Imd signaling dependent on the JNK signaling pathway

FoxO is one of the transcription factors that execute effects of JNK pathway activation (Essers et al., 2004; Wang et al., 2005). Therefore, we evaluated whether FoxO, the sole ortholog of the

epithelial thickening, which is lower but clearly present (Figure 4C). Nevertheless, these results demonstrated that JNK signaling is required to enable airway hyper- and metaplasia in response to Imd pathway activation. Furthermore, we wanted to find out whether *PGRP-LC* overexpression is sufficient to activate the JNK pathway in the tracheae. Therefore, we analyzed phosphorylation of basket (JNK). Immunostaining analyses revealed only marginal staining in non-induced control airways (Figure 5C), whereas a strong increase in pJNK in

Figure 6. The JNK branch of the Imd signaling pathway mediates FoxO (forkhead transcription factor of the O subgroup) translocation in the airway epithelium

(A) Fluorescence image of second-instar larva from crosses between a promotor-*foxo*-Gal4 strain and a UAS-*gfp* strain (white arrowheads mark airways). Scale bar, 500 μm.

(B–E) Fluorescence images of second-instar larvae overexpressing *gfp*-tagged *foxo* (B); overexpressing *gfp*-tagged *foxo* and *PGRP-LC* simultaneously (C); overexpressing *gfp*-tagged *foxo*, *PGRP-LC*, and *bsk*^{DN} simultaneously (D; UAS-*bsk*^{DN}), or overexpressing *gfp*-tagged *foxo*, *PGRP-LC*, and *bsk*-RNAi simultaneously (E; UAS-*bsk*-RNAi) in the tracheae. White arrowheads mark airways, red arrows indicate translocation events, and white arrows indicate melanization. Scale bars, 500 μm (top images) and 50 μm (bottom images).

(F) A quantitative analysis of the nuclear translocation behavior of FoxO was performed with ImageJ.

(G and H) The effects of short cold exposure (2 h, 4°C, right image line; the left image line shows controls) were analyzed in *Drosophila* larvae (G) as well as in human airway epithelial cells (H). The translocation behavior of eFP-tagged transcription factors targeted to the *Drosophila* trachea (*foxo-gfp*, top; *dorsal-gfp*, center; *relish-yfp*, bottom) is shown (G). In (H), immunohistochemical analyses of A549 cells using α-FoxO1 antibodies are shown (α-FoxO1, top; DAPI, center; merge of α-FoxO1 and DAPI, bottom). Scale bars, 100 μm (G) and 25 μm (H).

(I) The outcome of severe hypoxia on survival of *foxo*-deficient (*foxo*$^{21/21}$) as well as control flies. They were subjected to 24 h of hypoxia (1% O$_2$), and survival was measured 24 h later.

Data show mean values ± SD. n = 20 (F), n = 11 (I), t test, **p < 0.01.

---

forkhead-box subgroup O family in *Drosophila*, is involved in airway remodeling because of JNK activation. Using a *foxo*-promoter-Gal4 strain, we demonstrated that the *foxo* gene is highly expressed throughout the airways of *Drosophila* larvae (Figure 6A, white arrowheads). To test whether Imd pathway activation affects FoxO signaling, we used *ppk4*-Gal4, UAS-*foxo-gfp* flies and analyzed the subcellular localization and intracellular trafficking of FoxO-GFP in the airway epithelium. As expected, in the absence of any treatment or stimulation, FoxO-GFP was present exclusively in the cytoplasm of airway epithelial cells (Figure 6B, white arrowheads). However, concurrent overexpression of *PGRP-LC* and *foxo-gfp* provoked organ-wide nuclear translocation of FoxO-GFP (Figure 6C, red arrows), indicating that FoxO translocation is triggered by Imd signaling. So far, we could conclude that strong and persistent Imd activation triggered by forced *PGRP-LC* or *PGRP-LE* overexpression induced JNK signaling and FoxO activation in the airway epithelium of *Drosophila* larvae. However, it was still unclear whether FoxO and JNK activation are part of the same signaling system. To clarify this, we generated fly strains in which *PGRP-LC* and *foxo-gfp* were overexpressed concurrent with *bsk*-RNAi or *bsk*^{DN} in the airway epithelium. Regardless of whether

JNK signaling was impaired by *bsk*-RNAi or by co-expression of *bsk*^{DN}, nuclear FoxO translocation was abolished completely in airway epithelial cells lacking active JNK signaling while experiencing Imd activation (Figures 6D and 6E). A quantitative evaluation of these results using the fluorescent signals in nuclear and cytosolic regions of airway epithelial cells revealed only for the ectopic overexpression of *PGRP-LC* without concurrent reduction of JNK signaling an increased nuclear-to-cytosolic signal ratio. On the other hand, those flies experiencing simultaneous overexpression of *PGRP-LC* and *bsk*^{DN} or *bsk*-RNAi showed ratios at levels similar to as observed in the controls (Figure 6F). These results demonstrate that Imd signaling in the airway epithelium drives nuclear FoxO translocation through activation of the JNK pathway. Moreover, we also observed melanization in the trachea in response to *PGRP-LC* overexpression, regardless of whether the JNK pathway was impaired (Figures 6C–6E white arrows). This shows that the PGRP-LC induced melanization response is independent of the JNK pathway.

To test whether other stressors could elicit similar responses (i.e., inducing translocation and, therefore, activation of relevant transcription factors in the airways), we used a short period of

cold treatment (2 h, 4°C) as a model stressor, which has been linked repeatedly to chronic lung disease and can lead to exacerbation of asthma and COPD (Hansel et al., 2016; Seys et al., 2019). Therefore, we used eFP (enhanced fluorescent protein)-tagged transcription factors targeted to the larval airways and could show that this cold treatment induced almost complete nuclear translocation of FoxO in comparison with controls, where no signs of nuclear localization were observed (Figure 6G). In contrast, we did not observe any signal of nuclear translocation for the transcription factors Dorsal (*dl*) and Relish (*rel*) (Figure 6G). We also analyzed the human cell line A549, which originates from alveolar cells. Here we used immunohistochemistry with α-FoxO1 antiserum and could show that 2 h of cold exposure induced almost complete nuclear translocation of FoxO1, whereas its localization under control (unstressed) conditions was mostly restricted to the cytosol (Figure 6H). Finally, we evaluated whether the presence of FoxO factors had a physiologically relevant outcome that could be attributed to airborne signals. Here, we subjected *foxo*-deficient (*foxo*[21/21]) as well as control flies to hypoxia (1 day, 1% O_2) and could show that *foxo*-deficient flies were significantly more susceptible to this intervention because their survival rate was significantly lower (Figure 6I).

The JNK target gene FoxO is essential for transmission of Imd-induced epithelial remodeling

Next we evaluated whether FoxO activation alone was sufficient for induction of the remodeling phenotype. Expression of a constitutively active isoform of *foxo* resulted in early larval death because of massive malformation of the airways. Thus, we ectopically overexpressed the wild-type form of *foxo* in the airway epithelium. As in *relD*-overexpressing airways (Figure 4B), expression of the AMP genes *drosomycin* and *diptericin* was elevated (Figure S3). Moreover, compared with matching controls, (Figures 7A and 7C), *foxo*-overexpressing airways showed morphological changes consistent with those observed in *PGRP-LC*-overexpressing ones, comprising loss of epithelial regularity (Figure 7B), airway deformation (Figure 7D, black arrow) and epithelial thickening (Figures 7D and 7E). Immunofluorescence analyses suggested that epithelial thickening was also caused by excessive proliferation of epithelial cells (Figures 7F and 7G) and a structural change of these cells, as exemplified by an increase in the nuclear sizes of epithelial cells by a factor of 1.6 (Figures 7H and 7I).

To determine whether FoxO activation is not only sufficient but also necessary for these phenotypic alterations, we activated the Imd signaling pathway in *foxo*-RNAi (*foxo*[RNAi]) or *foxo*-deficient (*foxo*[21/21]) backgrounds. Although ectopic overexpression of *foxo* or *PGRP-LC* significantly increased epithelial thickness (Figures 7E and 7J), overexpression of *PGRP-LC* in a *foxo*-deficient background resulted in animals with almost normal airways, irrespective of whether endogenous *foxo* expression was reduced by RNAi or abolished completely (*foxo*[21/21]; Figure 7J).

DISCUSSION

Using a *Drosophila* model of airway remodeling, we demonstrate that chronic activation of the epithelial immune system leads to substantial structural changes in the respiratory tract that are associated with dysfunction of the organ. These induced structural changes comprise meta- and hyperplastic transformations of airway epithelial cells. We were able to detect these induced structural changes at all life stages of *Drosophila*, even in adults, which experienced only a short phase of Imd pathway activation. For technical reasons, however, we performed the more in-depth mechanistic analyses on larvae. Local airway remodeling processes in response to strong immune activation have already been shown in the fly's airways (Wagner et al., 2009). This reaction appears to be very specific because other stressors, such as chronic cigarette smoke exposure, did not induce such a response (Prange et al., 2018). Because deregulation of NF-κB signaling in airway epithelial cells of mice is sufficient to induce lung pathology-associated structural changes in, for example, asthma models (Broide et al., 2005; Pantano et al., 2008), it was surprising to see that only a small part of the structural changes observed in the *Drosophila* airway remodeling model could be attributed directly to epithelial NF-κB signaling. In contrast, we observed that, in the *Drosophila* airway system, most of the structural changes that result from chronic epithelial immune activation depend on JNK signaling involving the transcription factor FoxO. This is possible because Tak1 intertwines two signaling pathways, the classical Imd one, which leads to activation of the NF-κB factor Relish, and the JNK signaling pathway. This bifurcation of signaling, which allows activation of NF-κB and JNK signaling downstream of Tak1, is not restricted to *Drosophila*; in many mammals (including humans), Tak1 also acts as an intracellular hub molecule activating NF-κB- and JNK-dependent signaling processes (Sabio and Davis, 2014; Shim et al., 2005).

JNK signaling is associated with a number of different chronic lung diseases, including lung fibrosis, COPD, asthma, and lung cancer (Eurlings et al., 2017; Eynott et al., 2003; Khatlani et al., 2007; van der Velden et al., 2016). Excessive activation of JNK signaling is correlated with epithelial-mesenchymal transition processes in the lung (Willis and Borok, 2007), which makes JNK signaling a reasonable target for specific intervention strategies (van der Velden et al., 2016). Airway epithelial JNK signaling is activated by a variety of stressors, including infection and UV radiation, and has a central role in lung tissue repair mechanisms (Crosby and Waters, 2010).

Downstream of JNK signaling, transcription factors such as AP1 and FoxO execute the physiological effects of pathway activation. In the present study, we demonstrated that FoxO is necessary and sufficient to induce airway remodeling in response to chronic Imd pathway activation. We assume that the complex reactions leading to these structural changes are part of a FoxO-dependent survival program (Luo et al., 2005) that is usually required to maintain tissue homeostasis, especially in the case of locally occurring damage (Pasparakis, 2008, 2009). Such tissue damage can be healed by cell division and cell migration in the epithelium (Simnett and Fisher, 1976), which requires hyper- and metaplasia of airway epithelial cells. Although hyper- and metaplasia are inevitable for regeneration, such changes can trigger development of chronic lung diseases and cancer (Karin and Greten, 2005). In *Drosophila*, thickening or swelling of the epithelial cell layer, caused by hyper- and
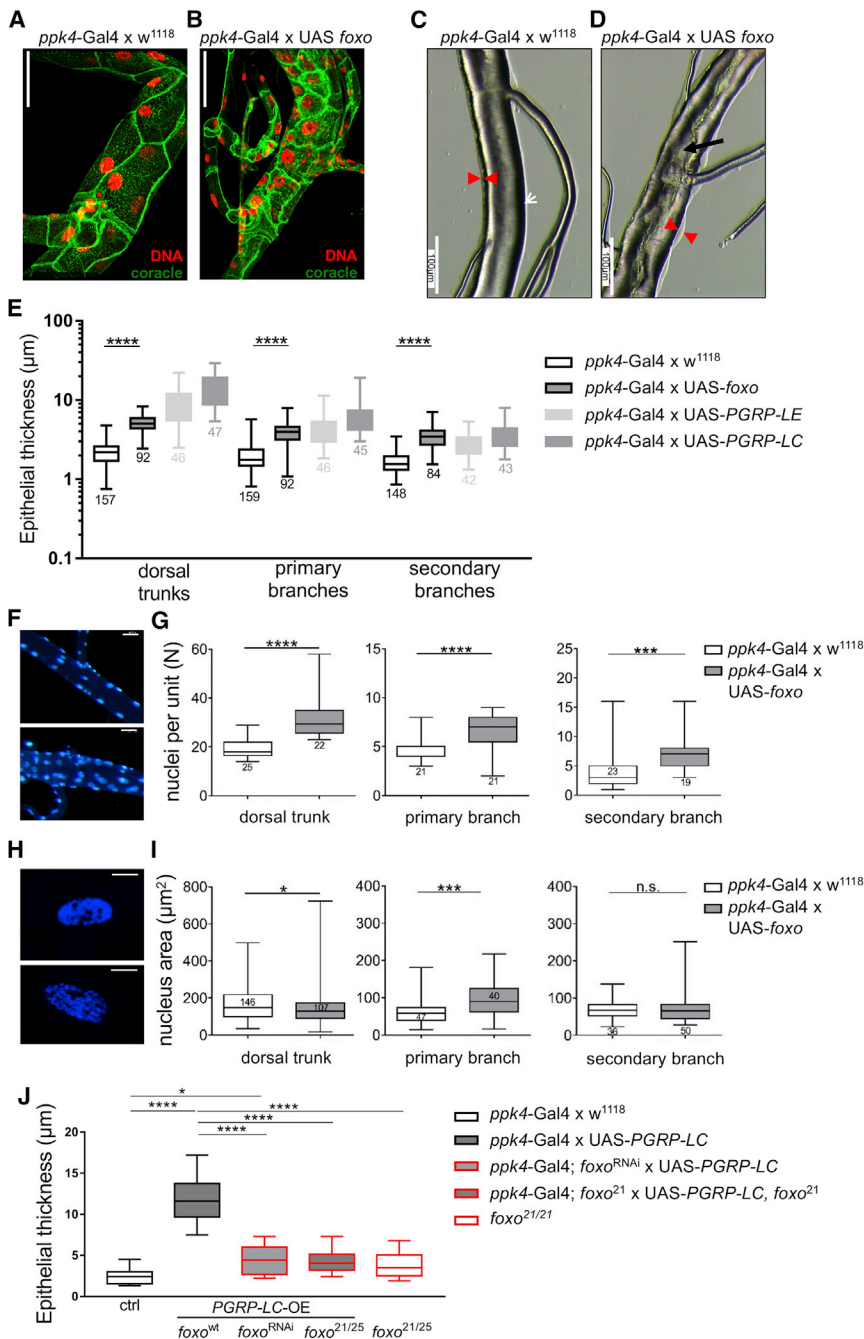
Figure 7. The JNK target gene *foxo* is necessary to mediate Imd-induced epithelial remodeling

(A and B) Confocal fluorescence microscopy images of DAPI- and anti-coracle-stained airways from *foxo*-overexpressing larvae (B) and matching controls (A). Scale bars, 100 μm.

(C and D) Low-magnification light microscopy analyses of airways experiencing *foxo* overexpression (D) or not (C). Red arrowheads, epithelial thickness; black arrow, inner air conducting space. Scale bars, 100 μm.

(E) Quantification of epithelial thicknesses in different airway branching generations of larvae experiencing *foxo* overexpression.

(F) Fluorescence images of DAPI-stained dorsal trunks derived from *foxo*-overexpressing airways (bottom image) and matching controls (top image). Scale bars, 50 μm.

(G) Quantification of cell nuclei in dorsal trunks and primary and secondary branches of *foxo*-overexpressing airways.

(H) Fluorescence images of DAPI-stained epithelial nuclei from dorsal trunks of *foxo*-overexpressing airways (bottom image) and matching controls (top image). Scale bar, 10 μm.

(I) Quantification of nuclear sizes in dorsal trunks and primary and secondary branches from *foxo*-overexpressing airways.

(J) Quantitative evaluation of epithelial thicknesses in dorsal trunks overexpressing *PGRP-LC* in a wild-type genetic background or in a foxo-deficient background.

Data show mean values ± SEM. n ≥ 42 (E), n ≥ 19 (G and I), n ≥ 12 (J) two-tailed Mann-Whitney U test: $*p < 0.01$, $***p < 0.001$, $****p < 0.0001$. Values calculated from at least n = 12 animals. Significant differences to controls are indicated by one-way ANOVA, F = 51.6, $*p < 0.05$, $***p < 0.001$, $****p < 0.0001$.

metaplasia of epithelial cells, is the major pathological characteristic, something that is also observed in severe forms of asthma in humans (Cohen et al., 2007). This reaction occurs naturally in the fly's airway epithelium in response to strong infection, but usually it remains local, avoiding the pathological effects observed in response to organ-wide activation of these systems (Wagner et al., 2009).

FoxO factors act as sentinels for a wide array of stressors in airway epithelial cells in *Drosophila* and vertebrates (Pantano et al., 2008; Roeder et al., 2009; Salih and Brunet, 2008).

They also operate as regulators of innate immunity in respiratory epithelial cells, especially in response to bacterial stimuli (Seiler et al., 2013). FoxO factors in general and FoxO1 especially appear to be highly relevant for wound healing processes, which is consistent with our observations (Ponugoti et al., 2013). In the *Drosophila* epidermis, reduced FoxO signaling is important for effective wound repair (Kakanj et al., 2016), whereas the results obtained in murine models remain conflicting, showing better wound healing by reduced FoxO signaling (Mori et al., 2014) or exactly the opposite (Ponugoti et al., 2013). Deregulation of FoxO1-mediated signaling in specific cell populations is associated with various chronic inflammatory diseases (Wilhelm et al., 2016), including rheumatoid arthritis (Grabiec et al., 2015) and pulmonary hypertension (Savai et al., 2014). We could also demonstrate that FoxO signaling, presumably in the airways, is necessary to cope with highly

stressful conditions, such as severe hypoxia. Furthermore, FoxO3A has been detected in its activated form in airway epithelial cells of individuals with COPD, cystic fibrosis, or ARDS (acute respiratory distress syndrome) pneumonia (Seiler et al., 2013). In contrast, a different study found reduced activated FoxO3A levels in airway epithelial cells from individuals with COPD (Ganesan et al., 2013), further supporting an important role of this FoxO factor in this context, but also reveals our insufficient knowledge of the underlying mechanisms.

Cellular sentinels such as FoxO always carry the risk of reacting inappropriately, especially when different stimuli act in a temporally coordinated way. A certain level of JNK/FoxO activation/deregulation caused by chronic input can remain inconspicuous over a long time, but an additional stressor, such as an infection, might cause activation above the threshold, leading to remodeling of the airways (Broide, 2008; Cheng et al., 2007; Hart et al., 1998; Holgate, 2007b). Taking into account this highly important role of the JNK/FoxO axis for disease-associated remodeling processes, utilizing these signaling systems as intervention targets in chronic lung diseases is an emerging but highly promising field (Al-Tamari et al., 2018; Defnet et al., 2020; Eurlings et al., 2017; van der Velden et al., 2016).

Activation of epithelial Imd signaling in the fly induced substantial structural changes comprising epithelial hyper- and metaplasia that resemble those observed in human inflammatory lung diseases (Ganesan and Sajjan, 2013; Grainge and Davies, 2013). Moreover, we demonstrated that these structural changes do not depend on NF-κB signaling but are driven by cell-autonomous JNK signaling and the activity of its downstream-acting transcription factor FoxO. Given the central role of airway epithelial cells in controlling the pathophysiological state of the airways in chronic inflammatory lung diseases, our findings enhance the understanding of how chronic activation of the airway innate immune system results in disease-associated structural changes. This perspective should lead to consideration of treatment strategies that explicitly focus on the remodeling processes and, in particular, address the JNK-FoxO axis as a pharmacological target.

Limitations of study

It has to be kept in mind that, although the *Drosophila* model has many outstanding advantages for analysis of structural changes in the respiratory tract, some important aspects of airway remodeling in humans cannot be represented at all or only insufficiently. These include, in particular, structural changes that affect subepithelial parts of the airways, such as submucosal collagen deposition, thickening of smooth muscles, and angiogenesis. However, our main focus remains the role of the epithelium in the pathogenesis of chronic inflammatory lung diseases, which can be modeled perfectly with the fly. Moreover, it should be considered that relevant signaling pathways, as characterized in this paper, take on different functions in different contexts. This is especially true for experiments in which developmental processes cannot be explicitly excluded. For this reason, such studies should be conducted so that the importance of development can be estimated or, better yet, excluded.

STAR★METHODS

Detailed methods are provided in the online version of this paper and include the following:

- KEY RESOURCES TABLE
- RESOURCE AVAILABILITY
  - Lead contact
  - Materials availability
  - Data and code availability
- EXPERIMENTAL MODEL AND SUBJECT DETAILS
  - Experimental models: *Drosophila*
  - Cross-breedings
  - Experimental models: Cell lines
- METHOD DETAILS
  - RNA extraction and quantitative RT-PCR analysis
  - Measuring the number of terminal branches in *Drosophila* larvae
  - Measuring epithelial thickness, size, and number of nuclei in tracheal specimen
  - Immobilization of larvae and *in vivo* imaging of airways and hypoxia treatment of adult flies
  - Preparation, fixation, and staining for imaging of tracheal cross sections by TEM
  - Preparation, fixation, and immunofluorescence staining for imaging of larval and adult airways
  - Preparation, fixation, and immunofluorescence staining for imaging of human A549 cells
- QUANTIFICATION AND STATISTICAL ANALYSIS

AUTHOR CONTRIBUTIONS

Experimental design/discussion, C.W., K.U., C.V., K.I., N.S., H.H., and T.R.; preparation and performance of experiments and data analysis, C.W., K.U., M.T., C.V., K.I., A.A., J.B., X.N., C.F., M.W., M.K., A.R.K., M.P., P.K., H.F., U.M.Z., C.B.S.-W., and H.G.; manuscript preparation, C.W., K.U., H.H., P.P., H.R., and T.R. All authors agreed on the contents, including the author list and author contribution statements.

DECLARATION OF INTERESTS

The authors declare no competing interests.

REFERENCES

Adam, D., Roux-Delrieu, J., Luczka, E., Bonnomet, A., Lesage, J., Mérol, J.C., Polette, M., Abély, M., and Coraux, C. (2015). Cystic fibrosis airway epithelium remodelling: involvement of inflammation. J. Pathol. *235*, 408–419.

Akhouayri, I., Turc, C., Royet, J., and Charroux, B. (2011). Toll-8/Tollo negatively regulates antimicrobial response in the Drosophila respiratory epithelium. PLoS Pathog. *7*, e1002319.

Al-Tamari, H.M., Dabral, S., Schmall, A., Sarvari, P., Ruppert, C., Paik, J., DePinho, R.A., Grimminger, F., Eickelberg, O., Guenther, A., et al. (2018). FoxO3 an important player in fibrogenesis and therapeutic target for idiopathic pulmonary fibrosis. EMBO Mol. Med. *10*, 276–293.

Bosch, J.A., Tran, N.H., and Hariharan, I.K. (2015). CoinFLP: a system for efficient mosaic screening and for visualizing clonal boundaries in Drosophila. Development *142*, 597–606. https://doi.org/10.1242/dev.114603.

Brand, A.H., and Perrimon, N. (1993). Targeted gene expression as a means of altering cell fates and generating dominant phenotypes. Development *18* (2), 401–415.

Broide, D.H. (2008). Immunologic and inflammatory mechanisms that drive asthma progression to remodeling. J. Allergy Clin. Immunol. *121*, 560–570, quiz 571–572.

Broide, D.H., Lawrence, T., Doherty, T., Cho, J.Y., Miller, M., McElwain, K., McElwain, S., and Karin, M. (2005). Allergen-induced peribronchial fibrosis and mucus production mediated by IkappaB kinase beta-dependent genes in airway epithelium. Proc. Natl. Acad. Sci. USA *102*, 17723–17728.

Camelo, A., Dunmore, R., Sleeman, M.A., and Clarke, D.L. (2014). The epithelium in idiopathic pulmonary fibrosis: breaking the barrier. Front. Pharmacol. *4*, 173.

Chen, F., and Krasnow, M.A. (2014). Progenitor outgrowth from the niche in Drosophila trachea is guided by FGF from decaying branches. Science *343* (6167), 186–189.

Cheng, D.S., Han, W., Chen, S.M., Sherrill, T.P., Chont, M., Park, G.Y., Sheller, J.R., Polosukhin, V.V., Christman, J.W., Yull, F.E., and Blackwell, T.S. (2007). Airway epithelium controls lung inflammation and injury through the NF-kappa B pathway. J. Immunol. *178*, 6504–6513.

Cohen, L., e, X., Tarsi, J., Ramkumar, T., Horiuchi, T.K., Cochran, R., DeMartino, S., Schechtman, K.B., Hussain, I., Holtzman, M.J., and Castro, M.; NHLBI Severe Asthma Research Program (SARP) (2007). Epithelial cell proliferation contributes to airway remodeling in severe asthma. Am. J. Respir. Crit. Care Med. *176*, 138–145.

Crosby, L.M., and Waters, C.M. (2010). Epithelial repair mechanisms in the lung. Am. J. Physiol. Lung Cell. Mol. Physiol. *298*, L715–L731.

Defnet, A.E., Hasday, J.D., and Shapiro, P. (2020). Kinase inhibitors in the treatment of obstructive pulmonary diseases. Curr. Opin. Pharmacol. *51*, 11–18.

DiAngelo, J.R., Bland, M.L., Bambina, S., Cherry, S., and Birnbaum, M.J. (2009). The immune response attenuates growth and nutrient storage in Drosophila by reducing insulin signaling. Proc Natl Acad Sci U S *A106*,, 20853–20858. https://doi.org/10.1073/pnas.0906749106.

Essers, M.A., Weijzen, S., de Vries-Smits, A.M., Saarloos, I., de Ruiter, N.D., Bos, J.L., and Burgering, B.M. (2004). FOXO transcription factor activation by oxidative stress mediated by the small GTPase Ral and JNK. EMBO J. *23*, 4802–4812.

Eurlings, I.M., Reynaert, N.L., van de Wetering, C., Aesif, S.W., Mercken, E.M., de Cabo, R., van der Velden, J.L., Janssen-Heininger, Y.M., Wouters, E.F., and Dentener, M.A. (2017). Involvement of c-Jun N-Terminal Kinase in TNF-α-Driven Remodeling. Am. J. Respir. Cell Mol. Biol. *56*, 393–401.

Eynott, P.R., Nath, P., Leung, S.Y., Adcock, I.M., Bennett, B.L., and Chung, K.F. (2003). Allergen-induced inflammation and airway epithelial and smooth muscle cell proliferation: role of Jun N-terminal kinase. Br. J. Pharmacol. *140*, 1373–1380.

Fehrenbach, H. (1995). Egg shells of Lepidoptera - Fine structure and phylogenetic implications. Zoologischer Anzeiger *234*, 19–41.

Ganesan, S., and Sajjan, U.S. (2013). Repair and Remodeling of airway epithelium after injury in Chronic Obstructive Pulmonary Disease. Curr. Respir. Care Rep. *2*.

Ganesan, S., Unger, B.L., Comstock, A.T., Angel, K.A., Mancuso, P., Martinez, F.J., and Sajjan, U.S. (2013). Aberrantly activated EGFR contributes to enhanced IL-8 expression in COPD airways epithelial cells via regulation of nuclear FoxO3A. Thorax *68*, 131–141.

Grabiec, A.M., Angiolilli, C., Hartkamp, L.M., van Baarsen, L.G., Tak, P.P., and Reedquist, K.A. (2015). JNK-dependent downregulation of FoxO1 is required to promote the survival of fibroblast-like synoviocytes in rheumatoid arthritis. Ann. Rheum. Dis. *74*, 1763–1771.

Grainge, C.L., and Davies, D.E. (2013). Epithelial injury and repair in airways diseases. Chest *144*, 1906–1912.

Hansel, N.N., McCormack, M.C., and Kim, V. (2016). The Effects of Air Pollution and Temperature on COPD. COPD *13*, 372–379.

Hanson, M.A., Dostalova, A., Ceroni, C., Poidevin, M., Kondo, S., and Lemaitre, B. (2019). Synergy and remarkable specificity of antimicrobial peptides in vivo using a systematic knockout approach. eLife *8*, e44341.

Hart, L.A., Krishnan, V.L., Adcock, I.M., Barnes, P.J., and Chung, K.F. (1998). Activation and localization of transcription factor, nuclear factor-kappaB, in asthma. Am. J. Respir. Crit. Care Med. *158*, 1585–1592.

Hedengren, M., Asling, B., Dushay, M.S., Ando, I., Ekengren, S., Wihlborg, M., and Hultmark, D. (1999). Relish, a central factor in the control of humoral but not cellular immunity in Drosophila. Mol. Cell *4*, 827–837.

Hiemstra, P.S., McCray, P.B., Jr., and Bals, R. (2015). The innate immune function of airway epithelial cells in inflammatory lung disease. Eur. Respir. J. *45*, 1150–1162.

Holgate, S.T. (2007a). Epithelium dysfunction in asthma. J. Allergy Clin. Immunol. *120*, 1233–1244, quiz 1245–1246.

Holgate, S.T. (2007b). The epithelium takes centre stage in asthma and atopic dermatitis. Trends Immunol. *28*, 248–251.

Junger, M.A., Rintelen, F., Stocker, H., Wasserman, J.D., Vegh, M., Radimerski, T., Greenberg, M.E., and Hafen, E. (2003). The Drosophila forkhead transcription factor FOXO mediates the reduction in cell number associated with reduced insulin signaling. J Biol *2*, 20. https://doi.org/10.1186/1475-4924-2-20.

Kakanj, P., Moussian, B., Grönke, S., Bustos, V., Eming, S.A., Partridge, L., and Leptin, M. (2016). Insulin and TOR signal in parallel through FOXO and S6K to promote epithelial wound healing. Nat. Commun. *7*, 12972.

Kallsen, K., Zehethofer, N., Abdelsadik, A., Lindner, B., Kabesch, M., Heine, H., and Roeder, T. (2015). ORMDL deregulation increases stress responses and modulates repair pathways in Drosophila airways. J. Allergy Clin. Immunol. *136*, 1105–1108.

Karin, M., and Greten, F.R. (2005). NF-kappaB: linking inflammation and immunity to cancer development and progression. Nat. Rev. Immunol. *5*, 749–759.

Khatlani, T.S., Wislez, M., Sun, M., Srinivas, H., Iwanaga, K., Ma, L., Hanna, A.E., Liu, D., Girard, L., Kim, Y.H., et al. (2007). c-Jun N-terminal kinase is activated in non-small-cell lung cancer and promotes neoplastic transformation in human bronchial epithelial cells. Oncogene *26*, 2658–2666.

Lambrecht, B.N., and Hammad, H. (2012). The airway epithelium in asthma. Nat. Med. *18*, 684–692.

Levine, B.D., and Cagan, R.L. (2016). Drosophila Lung Cancer Models Identify Trametinib plus Statin as Candidate Therapeutic. Cell Rep. *14*, 1477–1487.

Liu, L., Johnson, W.A., and Welsh, M.J. (2003). Drosophila DEG/ENaC pick-pocket genes are expressed in the tracheal system, where they may be involved in liquid clearance. Proc. Natl. Acad. Sci. USA *100*, 2128–2133.

Luo, J.L., Kamata, H., and Karin, M. (2005). The anti-death machinery in IKK/NF-kappaB signaling. J. Clin. Immunol. *25*, 541–550.

McGuire, S.E., Le, P.T., Osborn, A.J., Matsumoto, K., and Davis, R.L. (2003). Spatiotemporal rescue of memory dysfunction in Drosophila. Science *302*, 1765–1768.

Mori, R., Tanaka, K., de Kerckhove, M., Okamoto, M., Kashiyama, K., Tanaka, K., Kim, S., Kawata, T., Komatsu, T., Park, S., et al. (2014). Reduced FOXO1 expression accelerates skin wound healing and attenuates scarring. Am. J. Pathol. *184*, 2465–2479.

Onfelt Tingvall, T., Roos, E., and Engström, Y. (2001). The imd gene is required for local Cecropin expression in Drosophila barrier epithelia. EMBO Rep. *2*, 239–243.

Pandey, U.B., and Nichols, C.D. (2011). Human disease models in Drosophila melanogaster and the role of the fly in therapeutic drug discovery. Pharmacol. Rev. *63*, 411–436.

Pantano, C., Ather, J.L., Alcorn, J.F., Poynter, M.E., Brown, A.L., Guala, A.S., Beuschel, S.L., Allen, G.B., Whittaker, L.A., Bevelander, M., et al. (2008). Nuclear factor-kappaB activation in airway epithelium induces inflammation and hyperresponsiveness. Am. J. Respir. Crit. Care Med. *177*, 959–969.

Pasparakis, M. (2008). IKK/NF-kappaB signaling in intestinal epithelial cells controls immune homeostasis in the gut. Mucosal Immunol. *1* (*Suppl 1*), S54–S57.

Pasparakis, M. (2009). Regulation of tissue homeostasis by NF-kappaB signalling: implications for inflammatory diseases. Nat. Rev. Immunol. *9*, 778–788.

Ponugoti, B., Xu, F., Zhang, C., Tian, C., Pacios, S., and Graves, D.T. (2013). FOXO1 promotes wound healing through the up-regulation of TGF-β1 and prevention of oxidative stress. J. Cell Biol. *203*, 327–343.

Prange, R., Thiedmann, M., Bhandari, A., Mishra, N., Sinha, A., Häsler, R., Rosenstiel, P., Uliczka, K., Wagner, C., Yildirim, A.O., et al. (2018). A *Drosophila* model of cigarette smoke induced COPD identifies Nrf2 signaling as an expedient target for intervention. Aging (Albany NY) *10*, 2122–2135.

Proud, D., and Leigh, R. (2011). Epithelial cells and airway diseases. Immunol. Rev. *242*, 186–204.

Roeder, T., Isermann, K., and Kabesch, M. (2009). Drosophila in asthma research. Am. J. Respir. Crit. Care Med. *179*, 979–983.

Roeder, T., Isermann, K., Kallsen, K., Uliczka, K., and Wagner, C. (2012). A Drosophila asthma model - what the fly tells us about inflammatory diseases of the lung. Adv. Exp. Med. Biol. *710*, 37–47.

Sabio, G., and Davis, R.J. (2014). TNF and MAP kinase signalling pathways. Semin. Immunol. *26*, 237–245.

Salih, D.A., and Brunet, A. (2008). FoxO transcription factors in the maintenance of cellular homeostasis during aging. Curr. Opin. Cell Biol. *20*, 126–136.

Savai, R., Al-Tamari, H.M., Sedding, D., Kojonazarov, B., Muecke, C., Teske, R., Capecchi, M.R., Weissmann, N., Grimminger, F., Seeger, W., et al. (2014). Pro-proliferative and inflammatory signaling converge on FoxO1 transcription factor in pulmonary hypertension. Nat. Med. *20*, 1289–1300.

Seiler, F., Hellberg, J., Lepper, P.M., Kamyschnikow, A., Herr, C., Bischoff, M., Langer, F., Schäfers, H.J., Lammert, F., Menger, M.D., et al. (2013). FOXO transcription factors regulate innate immune mechanisms in respiratory epithelial cells. J. Immunol. *190*, 1603–1613.

Seys, S.F., Lokwani, R., Simpson, J.L., and Bullens, D.M.A. (2019). New insights in neutrophilic asthma. Curr. Opin. Pulm. Med. *25*, 113–120.

Shim, J.H., Xiao, C., Paschal, A.E., Bailey, S.T., Rao, P., Hayden, M.S., Lee, K.Y., Bussey, C., Steckel, M., Tanaka, N., et al. (2005). TAK1, but not TAB1 or TAB2, plays an essential role in multiple signaling pathways in vivo. Genes Dev. *19*, 2668–2681.

Silverman, N., Zhou, R., Erlich, R.L., Hunter, M., Bernstein, E., Schneider, D., and Maniatis, T. (2003). Immune activation of NF-kappaB and JNK requires Drosophila TAK1. J. Biol. Chem. *278*, 48928–48934.

Simnett, J.D., and Fisher, J.M. (1976). Cell division and tissue repair following localized damage to the mammalian lung. J. Morphol. *148*, 177–184.

Takehana, A., Katsuyama, T., Yano, T., Oshima, Y., Takada, H., Aigaki, T., and Kurata, S. (2002). Overexpression of a pattern-recognition receptor, peptido-glycan-recognition protein-LE, activates imd/relish-mediated antibacterial defense and the prophenoloxidase cascade in Drosophila larvae. Proc. Natl. Acad. Sci. USA *99*, 13705–13710.

Tzou, P., Ohresser, S., Ferrandon, D., Capovilla, M., Reichhart, J.M., Lemaitre, B., Hoffmann, J.A., and Imler, J.L. (2000). Tissue-specific inducible expression of antimicrobial peptide genes in Drosophila surface epithelia. Immunity *13*, 737–748.

van der Velden, J.L., Ye, Y., Nolin, J.D., Hoffman, S.M., Chapman, D.G., Lahue, K.G., Abdalla, S., Chen, P., Liu, Y., Bennett, B., et al. (2016). JNK inhibition reduces lung remodeling and pulmonary fibrotic systemic markers. Clin. Transl. Med. *5*, 36.

Van Eerdewegh, P., Little, R.D., Dupuis, J., Del Mastro, R.G., Falls, K., Simon, J., Torrey, D., Pandit, S., McKenny, J., Braunschweiger, K., et al. (2002). Association of the ADAM33 gene with asthma and bronchial hyperresponsiveness. Nature *418*, 426–430.

Wagner, C., Isermann, K., Fehrenbach, H., and Roeder, T. (2008). Molecular architecture of the fruit fly's airway epithelial immune system. BMC Genomics *9*, 446.

Wagner, C., Isermann, K., and Roeder, T. (2009). Infection induces a survival program and local remodeling in the airway epithelium of the fly. FASEB J. *23*, 2045–2054.

Wang, M.C., Bohmann, D., and Jasper, H. (2005). JNK extends life span and limits growth by antagonizing cellular and organism-wide responses to insulin signaling. Cell *121*, 115–125.

Wark, P.A., Johnston, S.L., Bucchieri, F., Powell, R., Puddicombe, S., Laza-Stanca, V., Holgate, S.T., and Davies, D.E. (2005). Asthmatic bronchial epithelial cells have a deficient innate immune response to infection with rhinovirus. J. Exp. Med. *201*, 937–947.

Warmbold, C., Uliczka, K., Rus, F., Suck, R., Petersen, A., Silverman, N., Ulmer, A.J., Heine, H., and Roeder, T. (2013). Dermatophagoides pteronyssinus major allergen 1 activates the innate immune response of the fruit fly Drosophila melanogaster. J. Immunol. *190*, 366–371.

Whitsett, J.A., and Alenghat, T. (2015). Respiratory epithelial cells orchestrate pulmonary innate immunity. Nat. Immunol. *16*, 27–35.

Wilhelm, K., Happel, K., Eelen, G., Schoors, S., Oellerich, M.F., Lim, R., Zimmermann, B., Aspalter, I.M., Franco, C.A., Boettger, T., et al. (2016). FOXO1 couples metabolic activity and growth state in the vascular endothelium. Nature *529*, 216–220.

Willis, B.C., and Borok, Z. (2007). TGF-beta-induced EMT: mechanisms and implications for fibrotic lung disease. Am. J. Physiol. Lung Cell. Mol. Physiol. *293*, L525–L534.

Hwangbo, D.S., Gershman, B., Tu, M.P., Palmer, M., and Tatar, M. (2004). Drosophila dFOXO controls lifespan and regulates insulin signalling in brain and fat body. Nature 429, 562–566. https://doi.org/10.1038/nature02549

Pfaffl, M.W. (2001). A new mathematical model for relative quantification in real-time RT-PCR. Nucleic Acids Res 29, e45. https://doi.org/10.1093/nar/29.9.e45

Schramm, G., Bruchhaus, I., and Roeder, T. (2000). A simple and reliable 5'-RACE approach. Nucleic Acids Res *28*, E96. https://doi.org/10.1093/nar/28.22.e96

STAR★METHODS

KEY RESOURCES TABLE

REAGENT or RESOURCE	SOURCE	IDENTIFIER
Antibodies		
rabbit polyclonal anti JNK phospho antibody (pTPpY)	Promega	Cat # V7931 RRID:AB_430865
mouse polyclonal anti coracle	Developmental Studies Hybridoma Bank	Cat # SH30898 RRID:AB_1161642
rabbit IgG isotype control	Thermo Fisher Scientific	Cat # 02-6102 RRID:AB_2532938
rabbit polyclonal anti FoxO1a	abcam	Cat # ab39670 RRID:AB_732421
Alexa Fluor 488 goat polyclonal anti-mouse IgG	Thermo Fisher Scientific	Cat # A-11001 RRID:AB_2534069
Alexa Fluor 488 goat polyclonal anti-rabbit IgG	Thermo Fisher Scientific	Cat # A-11008 RRID:AB_143165
Experimental models: Organisms/strains		
Drosophila melanogaster w1118	BDSC	BDSC 3605 RRID:BDSC_3605
Drosophila melanogaster tubP-Gal80ts	BDSC	BDSC 7017 RRID:BDSC_7017
Drosophila melanogaster UAS-PGRP-LC	BDSC	BDSC 30919, BDSC 30918 RRID:BDSC_30919 RRID:BDSC_30918
Drosophila melanogaster UAS-PGRP-LE	BDSC	BDSC 33054 RRID:BDSC_33054
Drosophila melanogaster relE38	BDSC	BDSC 9458 RRID:BDSC_9458
Drosophila melanogaster UAS-gfp.valium10	BDSC	BDSC 35786 RRID:BDSC_35786
Drosophila melanogaster UAS-basketRNAi	BDSC	BDSC 32977 RRID:BDSC_32977
Drosophila melanogaster UAS-basketDN	BDSC	BDSC 9311 RRID:BDSC_9311
Drosophila melanogaster prom-foxo-Gal4	DGRC	DGRC 104412 RRID:DGGR_104412
Drosophila melanogaster UAS-foxo	BDSC	BDSC 9575 RRID:BDSC_9575
Drosophila melanogaster UAS-foxoRNAi	BDSC	BDSC 27656 RRID:BDSC_27656
Drosophila melanogaster UAS-gfp	BDSC	BDSC 32194 RRID:BDSC_32194
Drosophila melanogaster vvl-FLP/CyO, btl-moe-mRFP	BDSC	BDSC 64233 RRID:BDSC_64233
Drosophila melanogaster coinFLP-Gal4, UAS-2XEGFP	BDSC	BDSC 58751 RRID:BDSC_58751
Drosophila melanogaster GFP-balancer	BDSC	BDSC 4533 RRID:BDSC_4533
Drosophila melanogaster ppk4-Gal4	M. Welsh, Iowa, USA (Liu et al., 2003)	N/A
Drosophila melanogaster btl-Gal4	C. Klämbt, Münster, Germany	N/A
Drosophila melanogaster UAS-PGRP-LE/ drosomycin-gfp	S. Kurata, Tohoku Univ. Japan (Takehana et al., 2002)	N/A
Drosophila melanogaster UAS-relD	S. Cherry, Univ. Pennsylvania, USA (DiAngelo et al., 2009)	N/A
Drosophila melanogaster UAS-foxo-gfp	Wagner et al., 2009	N/A
Drosophila melanogaster UAS-dl-gfp	T. Ip, Univ. Massachussetts, Worcester, USA	N/A
Drosophila melanogaster UAS-rel-yfp	T. Ip, Univ. Massachussetts, Worcester, USA	N/A
Drosophila melanogaster UAS-foxo-TM	M. Tatar, Brown University, USA (Hwangbo et al., 2004)	N/A
Drosophila melanogaster foxo21/21	E. Hafen, Zuerich, Switzerland (Junger et al., 2003)	N/A
Drosophila melanogaster Sp(BL)/CyO; TM2/TM6	T. Stork, Univ. Massachusetts, Worcester, USA	N/A

Continued

REAGENT or RESOURCE	SOURCE	IDENTIFIER
Drosophila melanogaster btl-Gal4, tubP-Gal80ts, UAS-GFP	M. Leptin, Heidelberg, Germany	N/A
Experimental models: Cell lines		
A549	DSMZ	RRID: CVCL_0023
Software and algorithms		
GraphPad Prism version 7.00	https://www.graphpad.com/scientific-software/prism/	RRID: SCR_002798
cellSens Standard version 1.16	https://www.olympus-lifescience.com/en/software/cellsens/	RRID: SCR_014551
Leica Application Suite Advanced Fluorescence Software version 2.7.3.9723	https://www.leica-microsystems.com/products/microscope-software/p/leica-las-x-ls/	RRID: SCR_013673
ImageJ version 1.51j8	https://imagej.net/Welcome	RRID: SCR_003070

RESOURCE AVAILABILITY

Lead contact
Further information and requests for resources and reagents should be directed to and will be fulfilled by the Lead contact, Thomas Roeder (troeder@zoologie.uni-kiel.de).

Materials availability
Fly lines generated in this study are available from the Lead contact.

Data and code availability
The published article includes all datasets generated or analyzed during the study, this study did not generate any unique code.

EXPERIMENTAL MODEL AND SUBJECT DETAILS

Experimental models: *Drosophila*
The following transgenic *Drosophila* strains used were supplied by the Bloomington *Drosophila* Stock Center (BDSC) or the Kyoto *Drosophila* Genomics Resource Center (DGRC): w^{1118} (BDSC 3605), tubP-Gal80ts (BDSC 7017), UAS-PGRP-LC (BDSC 30919, BDSC 30918), UAS-PGRP-LE (BDSC 33054), relE38 (BDSC 9458), UAS-gfp.valium10 (BDSC 35786), UAS-basketRNAi (BDSC 32977), UAS-basketDN (BDSC 9311), prom-foxo-Gal4 (DGRC 104412), UAS-foxo (BDSC 9575), UAS-foxo (BDSC 9575), UAS-foxoRNAi (BDSC 27656), UAS-gfp (BDSC 32194), vvl-FLP/CyO, btl-moe-mRFP (BDSC 64233), coinFLP-Gal4, UAS-2XEGFP (BDSC 58751), GFP-balancer strain (BDSC 4533).

Additionally, the following stocks used were provided by scientists of the *Drosophila* research community: ppk4-Gal4 (M. Welsh, Iowa, USA; Liu et al., 2003), btl-Gal4 (C. Klämbt, Münster, Germany), UAS-PGRP-LE/drosomycin-gfp (drs-gfp; S. Kurata, Tohoku Univ. Japan; Takehana et al., 2002), UAS-relD (S. Cherry, Univ. Pennsylvania, USA; (DiAngelo et al., 2009), UAS-foxo-gfp (generated by ourselves; Wagner et al., 2009), UAS-dl-gfp and UAS-rel-yfp (T. Ip, Univ. Massachussetts, Worcester, USA), UAS-foxo-TM (M. Tatar, Brown University, USA; (Hwangbo et al., 2004)), foxo21/21 (E. Hafen, Zuerich, Switzerland; (Junger et al., 2003)), Sp(BL)/CyO; TM2/TM6 (T. Stork, Univ. Massachussetts, Worcester, USA), btl-Gal4, tubP-Gal80ts, UAS-GFP (M. Leptin, Heidelberg, Germany). If not described otherwise stocks and experimental flies were raised on standard cornmeal-agar medium at 25°C at a relative humidity of at least 60% with a 12 h:12 h light/dark cycle.

Cross-breedings
To induce expression of either genes of interest or GFP fusion proteins in larval airways we used the binary Gal4/UAS expression system (Brand and Perrimon, 1993). The tracheal TARGET system was established by generating a homozygous ppk4-Gal4(II)/tubP-Gal80ts(III) or by using a btl-Gal4, tubP-Gal80ts, UAS-GFP strain (McGuire et al., 2003), that could be crossed with the UAS-PGRP-LE/drosomycin-gfp (drs-gfp) strain. To generate the conventional Gal4/UAS and TARGET crossings, virgin females of the Gal4 strain were collected, at 3 days of age they were crossed with 5-7 days old males of the UAS strain. Experiments were performed with third instar (L3) larvae of the F1 generation, larvae were not sorted by gender.

To activate the TARGET system, larvae were maintained at 18°C (restrictive temperature) until reaching the desired developmental stage, then shifted to 28°C (permissive temperature) for at least 24 h. Animals permanently raised at 18°C served as controls.

Before crossing to ppk4-Gal4, the UAS-relD strain, balanced over a CyO chromosome, was rebalanced to a GFP-balancer strain (BDSC 4533) to visually identify third instar larvae carrying UAS-relD. UAS-PGRP-LE(II) was combined with UAS-gfp.valium10(III), UAS-basketRNAi(III), or UAS-basketDN(III) by using the multiple balancer strains Sp(BL)/CyO; TM2/TM6 (T. Stork, Univ. Massachusetts, Worcester, USA) to generate homozygous strains for (1) UAS-PGRP-LE(II); UAS-gfp.valium10(III); (2) UAS-PGRP-LE(II); UAS-basketR-NAi(III), or (3) UAS-PGRP-LE(II); UAS-basketDN(III). The same multiple balancer strains were used to generate the homozygous strains for ppk4-Gal4(II), relE38(III); UAS-PGRP-LC (II), relE38 (III); UAS-foxo-gfp(II), UAS-PGRP-LC(III); ppk4-Gal4(II), UAS-basketDN(III); ppk4-Gal4(II), UAS-basketRNAi(III); UAS-PGRP-LC(II), UAS-foxoRNAi(III); and UAS-PGRP-LC(II), foxo21/21(III).

The vvl-FLP/CyO; btl-moe.mRFP (BDSC 64233), tubP-Gal80ts and CoinFLP-Gal4, UAS-2xEGFP line was used for tracheal mosaic analyses. Ventral veins lacking (vvl) was expressed in larval tracheal clones that covered approximately 30 to 80% of the trachea ((Bosch et al., 2015); (Chen and Krasnow, 2014)).The genotype of the mosaic driver is vvl-FLP, CoinFLP-Gal4, UAS-2xEGFP/CyO; tub-Gal80ts (named vvl-coints). We crossed this driver line with UAS-PGRP-LC and the offspring (vvl-FLP, CoinFLP-Gal4, UAS-2xEGFP; tubP-Gal80ts/UAS-PGRP-LC) were raised at 18°C until reaching the L2 larvae stage. Animals were then transferred to 28°C to activate the UAS-PGRP-LC expression. The control is vvl-FLP, CoinFLP-Gal4, UAS-2xEGFP/; tubP-Gal80ts larvae, made by crossing vvl-coints with w[1118].

Experimental models: Cell lines

Type II alveolar epithelial cells A549 were cultured in RPMI (Biochrom, Berlin, Germany) supplemented with 10% fetal calf serum, 100 U/ml penicillin, and 100 μg/ml streptomycin at 37°C with 5% CO_2.

METHOD DETAILS

RNA extraction and quantitative RT-PCR analysis

For RNA isolation airways of surface-sterilized (5% sodium hypochloride), early third instar larvae were prepared manually in ice-cold sodium phosphate buffer saline (PBS). All adherent, non-tracheal tissue residuals were removed prior to purification. Between 20 and 25 pairs of airways were transferred to 350 μL lysis buffer (RA1) of the NucleoSpin RNA kit (Macherey-Nagel, Dueren, Germany). Airways were manually homogenized, and RNA was extracted according to the manufacturer's protocol, except that the incubation time for DNA cleavage by DNase I was extended to 30 min. Due to the limited yield of total RNA, ethanol/sodium acetate (final concentration 0.3 M; pH 5.5) precipitation was used for concentration. The RNA pellet was dried and resuspended in 20 μL RNase-free water. The RNA quality and quantity were determined on the Nanodrop ND-1000 UV/VIS spectrophotometer (VWR, Erlangen, Germany). CapFinder cDNA synthesis (Schramm et al., 2000) was performed for 1 h at 42°C using a first strand cDNA synthesis kit (Invitrogen Superscript III, Thermo Fisher Scientific/Life Technologies, Darmstadt, Germany) in a final volume of 10 μL as follows: 2 μL 5x first-strand buffer; 1 μL DTT (100 mM), 0.2 μL MnCl2 (40 mM), 1 μL dNTPs (10 mM), 0.5 μL OligodT25 primer (10 pmoL/μL; 5′-GAGAGAGGATCCAAGTACTAATAC GACTCACTATAGGGAGAT25A/ C/G-3′), 0.5 μL CapFinder primer (10 pmoL/μL, 5′-AAGCAGTGGTATCAACGCAGAG TGGCCAT TACGGCCrGrGrG-3′), 0.25 μL RNase OUT (40 units/μL; Thermo Fisher Scientific/Life Technologies, Darmstadt, Germany), 0.5 μL Superscript III (200 units/μL), 4 μL RNA (20-40 ng RNA). Subsequently, cDNA was amplified by LA-PCR (BD Biosciences Clontech PCR System Heidelberg, Germany) with the following reaction mixture: 5 μL 10x Advantage PCR-Puffer; 8 μL dNTPs (10 mM), 1 μL Oligo-dT7 primer (10 pmoL/μL, 5′-GAGAGAGGATCCAAGTACTAATACGACTCACTATAGG-3′); 1 μL CapFinder PCR primer (10 pmol/ μL; 5′-AAGCAGTGGTATCAACGCAG AGTGGCCATTACGGCCG-3′); 0.5 μL polymerase mix, 1 μL cDNA, and 33.5 μL PCR-grade water. LA-PCR was conducted under the following conditions: 30 cycles each with 95°C for 20 s, 58°C for 20 s, and 72°C for 2 min 30 s. Amplified cDNA was purified according to the information supplied by the manufacturer (JETQUICK PCR Purification Spin Kit; Genomed, Loehne, Germany) and the integrity and quality of the amplification products was checked by gel electrophoresis. Quantitative PCR (qPCR) was carried out with 1 μL amplified cDNA in 20 μL reaction volume of TAQurate Real-time PCR Master Mix according to the manufacturer's instructions (Epicenter Technologies, Biozym Scientific GmbH, Hessisch Oldendorf, Germany). A reaction mixture without cDNA served as negative control. Transcript levels were measured on a LightCycler 1.2 Instrument in 20 μL capillaries (Roche Diagnostics, Mannheim, Germany). The PCR cycling parameters were as follows: 30 s at 95°C, followed by 40 cycles of 95°C for 10 s, 58°C for 15 s, and 72°C for 15 s. Data collection was enabled at the extension step (72°C). The melting curve protocol followed with 15 s at 95°C and then 15 s each at 0.1°C increments between 62°C and 95°C. Data collection was enabled at each increment of the melting curve. Amplification and melting curves were generated by the LightCyler software version 3.5 (Roche Diagnostics, Mannheim, Germany). All samples were analyzed in duplicates/ triplicates, averaged and normalized against the housekeeping gene *actin 42A* or *rpl32.* Relative gene expression values were calculated by using the ΔΔCT-method (Pfaffl, 2001) and indicated in Figures 1A and 4B as n-fold expression differences compared to controls. At least three independent experiments were performed. The following primers were used: attA: 5′-CACAATGTGGTGGGTCAGG-3′, 5′-GGCACCATGACCAGCATT-3′; cecC: 5′-AAGATCTTCGTTTTCGTCGC-3′, 5′-GTTGCGCAATTCCCAGTC-3′; def: 5′-GCTATCGCTTTTGCTCTGCT-3′, 5′-GCCGCCTTTGAACCCCTTGG-3′; dipt: 5′-GCAATCGCT TCTACTTTGGC-3′, 5′-TAGGTGCTTCCCACTTTCCA-3′; dro: 5′- GTTCACCATCGTTTTCCTGC-3′, 5′-GGCAGCTTGAGTCAGG TGAT-3′; drs: 5′-GAGGAGGGACGCTCCAGT-3′, 5′-TTAGCATCCTTCGCACCAG-3′; mtch: 5′-CCACCGAGCTAAGATGCAA-3′, 5′-TGTTAACGACATCAGCAGTGTG-3′; act42A: 5′-TCGAAGCAAGAGTACGACGA-3′, 5′-CAATGGGTGTGTTCGATGAG-3′. rpl32: 5′-CCAGTCGGATCGATATGCTAA-3′, 5′-GTTCGATCCGTAACCGATGT-3′.

Measuring the number of terminal branches in *Drosophila* larvae

Third instar larvae were washed in PBS to remove remaining medium, before drying on a paper towel and transferring them into a drop of glycerol to glass slides. To kill the larvae, glass slides were incubated on a heating block with a temperature of 70°C for 20-30 s. Larvae were oriented with the dorsal side up and were covered with a coverslip. Images of the terminal branches were documented in the DIC channel of the Axio Imager.Z1 with Apo Tome (Zeiss, Oberkochen, Germany) using a 20x objective. To capture all terminal branches, Z stacks were generated. For the measurement, only terminal branches from the third dorsal segment were chosen. The numbers of terminal branches were counted using the AxioVision software (AxioVision SE64 Rel. 4.9, Zeiss, Oberkochen, Germany).

Measuring epithelial thickness, size, and number of nuclei in tracheal specimen

Epithelial thicknesses, nuclear sizes and numbers were measured in dorsal trunks, and primary and secondary branches of the seventh abdominal segment (A7). For this purpose, airways from third instar larvae were dissected and mounted in Roti®-Mount FluorCare DAPI (Carl Roth, Karlsruhe, Germany) or in ibidi Mounting Medium (ibidi, Planegg, Germany) mixed with ProLong Diamond Antifade Mountant with DAPI in a ratio of 1:1 (Thermo Fisher Scientific, Erlangen, Germany). Transmitted light images were taken with the SZX16 stereomicroscope (Olympus, Hamburg, Germany) using the SDFPLAPO2xPFC objective. Fluorescence images of DAPI-stained nuclei (blue) were made with the SZX2-FUV filter and the X-Cite 120 Iris UV lamp. The cellSens Standard software 1.16 (Olympus, Hamburg, Germany) or the AxioVision software (AxioVision SE64 Rel. 4.9, Zeiss, Oberkochen, Germany) were used to measure epithelial thicknesses, sizes and numbers of nuclei.

Immobilization of larvae and *in vivo* imaging of airways and hypoxia treatment of adult flies

In vivo analyses were performed with second and third instar larvae. Animals were washed in sodium phosphate buffer saline (1xPBS) at room temperature to remove remaining medium, placed in a drop of ibidi Mounting Medium (ibidi, Planegg, Germany) on a glass slide with the dorsal side up and covered with a coverslip. Glass slides were cooled down on a refrigerated block to physically immobilize the larvae and images were taken immediately to prevent cold stress. Nuclear translocation of FoxO-GFP, Dorsal-GFP, Relish-YFP, and GFP expression in prom-foxo-Gal4 x UAS-gfp larvae were analyzed under the SZX16 fluorescence stereomicroscope using SDF PLANAPO 1xPF/ 2xPFC objectives and the fluorescence filter SZX2-FGFP. Fluorescence images were taken by the DP72 camera and edited using the cellSens standard software 1.16 (Olympus, Hamburg, Germany). For stress tests early 3rd instar larvae were used. Temperature experiments were performed within medium. Animals subjected to cold shock were incubated at 4° for 2 h in medium.

Resistance toward severe hypoxia was tested in groups of 10 adults (5-7 days old) of controls (yw) and foxo21/21. Animals were subjected for 24h to 1% O_2 and their survival was quantified 1 day later.

Preparation, fixation, and staining for imaging of tracheal cross sections by TEM

Ripped early third instar larvae were fixed simultaneously with 1.5% glutaraldehyde and 2% osmium tetroxide in 0.1 M sodium cacodylate buffer for 90 min on ice (chemicals were provided by Serva Electrophoresis GmbH, Heidelberg, Germany; Sigma-Aldrich, Chemie GmbH, Taufkirchen, Germany and ChemPur, Karlsruhe, Germany). After rinsing with 0.1 M sodium cacodylate buffer, samples were post-fixed with 1% osmium tetroxide in 0.1 M sodium cacodylate buffer for 2 h, rinsed in the same buffer (4 × 5 min), washed in distilled water (2 × 5 min), and stained overnight *en bloc* in half-saturated uranyl acetate (Merck, Darmstadt, Germany). After rinsing with distilled water (4 × 5 min), samples were dehydrated through an ascending series of acetone (Carl Roth GmbH, Karlsruhe, Germany) (70%, 90%, 100% for each concentration; two times for 10 min), transferred into a 1:1-mixture of acetone and Araldite® (Serva Electrophoresis GmbH, Heidelberg, Germany) for 1 h, and then transferred into pure Araldite® overnight. After transfer into fresh resin, samples were polymerized at +60°C for 3 days. Ultrathin sections were cut on an Ultracut E (Reichart-Jung, Wien, Austria), collected on formvar-coated nickel grids, stained with lead citrate (Merck, Darmstadt, Germany), and analyzed using a Zeiss EM 900 (Zeiss, Oberkochen, Germany). Electron microscopy was performed as described earlier (Fehrenbach, 1995).

Preparation, fixation, and immunofluorescence staining for imaging of larval and adult airways

Early third instar larvae were washed first in PBS and then in 70% ethanol at room temperature, before they were placed in a block dish containing PBS. Larvae were opened longitudinally, the airways were exposed and all surrounding organs removed. For analysis of the adult tracheal system, the abdomen of adult flies was opened, and the majority of tissues was removed. Tissues were fixed in 3.5% paraformaldehyde (dissolved in PBS) at room temperature for 10 min, followed by washing in PBS. For immunostaining, samples were permeabilized with PBS/0.1% Triton X-100 and incubated with PBS/0.1% Triton X-100/10% normal goat serum (heat inactivated) for 30 min to block non-specific binding sites. The tissue was then incubated overnight with primary antibody solved in PBS/0.1% Triton X-100/10% NGS at 4°C. To visualize the airway epithelial cell-cell boundaries, exposed airways were stained for the septate junction marker coracle using the polyclonal mouse anti-coracle antibody (Developmental Studies Hybridoma Bank, Iowa, USA) in a dilution of 1:200. For the identification of JNK activation in the larval airway epithelium, polyclonal rabbit anti-JNK phospho-antibody (pTPpY) (Promega, Madison, USA; immunogenic sequence is 100% identical to *D. melanogaster* bsk/JNK) in a dilution of 1:100 was used. As isotype control, rabbit IgG isotype control (Thermo Fisher Scientific, Rockford, USA) was used in a dilution of 1:100. After primary antibody incubation, tissue was washed in PBS/0.1% Triton X-100 and incubated with secondary

antibodies Alexa Fluor® 488 goat anti-mouse IgG or Alexa Fluor® 488 goat anti-rabbit IgG (Thermo Fisher Scientific/Invitrogen, Karlsruhe, Germany) in a dilution of 1:300 (dissolved in PBS/0.1% Triton X-100) at room temperature for 1 h. Samples were washed twice in PBS/0.1% Triton X-100, then washed and stored in PBS. Airways were dissected in PBS, transferred to glass slides, embedded in mounting medium (a 1:1 mixture of ibidi Mounting Medium (ibidi, Planegg, Germany and ProLong Diamond Antifade Mountant with DAPI (Thermo Fisher Scientific, Erlangen, Germany), and sealed with a coverslip.

Tracheal specimens stained for coracle and DAPI were investigated using a TCS SP5 inverted confocal laser scanning microscope equipped with a 63x/1.32 HCX plan apochromat oil objective and argon and 405 diode lasers (Leica, Wetzlar, Germany). Images were edited using the LAS AF software. Airways, stained with the anti-pJNK antibody, were analyzed using a SZX16 fluorescence stereo-microscope with a DP72 camera, 2xPFC objective and fluorescence filters SZX2-FUV, SZX2-FGFP and SZX2-FGFPA (Olympus, Hamburg, Germany). Images were processed with the cellSens standard software (Olympus, Hamburg, Germany).

Preparation, fixation, and immunofluorescence staining for imaging of human A549 cells
Type II alveolar epithelial cells A549 were cultured in RPMI (Biochrom, Berlin, Germany) supplemented with 10% fetal calf serum, 100 U/ml penicillin, and 100 μg/ml streptomycin at 37°C with 5% CO2. Stress experiments were performed in μ-Slides (8 well ibiTreat, Ibidi, Martinsried, Germany) with $1.0x10^4$ cells per well, cells adhered to the slides for 24 h. Stress conditions were performed for two hours in supplemented medium at 4°C. Immediately afterward, cells were fixed with 3% paraformaldehyde, permeabilized with 0.25% Triton-X/PBS, blocked with 10% BSA/PBS and incubated with the primary antibody anti-FoxO1A antibody (rabbit polyclonal ChIP Grade, abcam, Cambridge, UK) and the secondary antibody Alexa Fluor® 488 goat anti-mouse IgG (Invitrogen, Karlsruhe, Germany). Nuclei were stained with Bisbenzimide H 33342 (Sigma-Aldrich, Deisenhofen, Germany). Images were taken with the TCS Sp5 inverted confocal laser scanning microscope and a 20x/0.70HC plan apochromatic oil-objective (Leica, Wetzlar, Germany). Images were edited using the Leica LAS AF Lite software and ImageJ software (Wayne Rasband, NIH) for quantitative analyses.

QUANTIFICATION AND STATISTICAL ANALYSIS

All experiments were repeated at least three times. Unpaired t test followed by Holm multiple comparison testing, two-tailed Mann Whitney U test, and one-way ANOVA were used to determine statistical significance. Statistical details for individual experiments can be found in the figure legends, the exact values of n are also indicated within the figures. Prism 7 (GraphPad) was used for graph editing and the statistical analyses, cellSens Standard 1.16 Software Olympus and Leica Application Suite Advanced Fluorescence Software (version 2.7.3.9723) Leica were used to take and edit photographs, image processing was done using ImageJ (version 1.51j8) software.